https://doi.org/10.5194/egusphere-2023-2447
Preprint. Discussion started: 17 November 2023

An improved estimate of inorganic iodine emissions from the ocean using a coupled surface microlayer box model

Ryan J. Pound[1], Lucy V. Brown[1], Mat J. Evans[1,2], and Lucy J. Carpenter[1]

[1]Wolfson Atmospheric Chemistry Laboratories, Department of Chemistry, University of York, York, YO10 5DD, UK
[2]National Centre for Atmospheric Science, University of York, York, YO10 5DD, UK

Correspondence: Ryan J. Pound (ryan.pound@york.ac.uk)

Abstract. Iodine at the ocean's surface impacts climate and health by removing ozone (O_3) from the troposphere both directly, via ozone deposition to seawater, and indirectly via the formation of iodine gases which are released into the atmosphere. Here we present a new box model of the ocean surface microlayer that couples oceanic O_3 dry deposition to inorganic chemistry to predict inorganic iodine emissions. This model builds on the previous work of Carpenter et al. (2013), improving both chemical and physical processes. This new box model predicts iodide depletion in the top few micrometres of the ocean surface, due to rapid chemical loss to ozone competing with replenishment from underlying water. From this box model, we produce parameterised equations for HOI and I_2 emissions which are implemented into the global chemical transport model GEOS-Chem. Compared to the previous model, inorganic iodine emissions from tropical waters decrease by as much as half, while higher latitude emissions increase by a factor of ∼10. Despite these large local changes, global total inorganic iodine emissions increased by only $\sim 4\%$ (2.83 Tg to 2.95 Tg) compared to the previous parameterization. This results in a negligible change in average tropospheric OH (<0.1%) and tropospheric methane lifetime (<0.1%). The annual mean tropospheric O_3 burden changes negligibly (an increase of 0.2% to 330 Tg), however, higher latitude surface O_3 concentrations decrease by as much as 15% with equatorial O_3 concentrations increasing by up to 10%.

1 Introduction

Iodine in the atmosphere and at the ocean-atmosphere interface is a large sink for tropospheric ozone (O_3). Dry deposition of O_3 to the ocean was thought to account for approximately one-third of the total O_3 loss to dry deposition (Ganzeveld et al., 2009), however, more recent work using more advanced representations of oceanic ozone dry deposition has revised this contribution down to ∼15% (Luhar et al., 2018; Pound et al., 2020). At the ocean surface, the reaction between O_3 and iodide (I^-) is thought to represent a significant fraction of this loss (Fairall et al., 2007; Carpenter et al., 2013). Most global models have a simplistic representation of oceanic O_3 dry deposition, which contributes to the uncertainty in tropospheric O_3 (Ganzeveld et al., 2009; Hardacre et al., 2015). Including a more advanced oceanic dry deposition scheme which incorporates the chemical

https://doi.org/10.5194/egusphere-2023-2447
Preprint. Discussion started: 17 November 2023

loss of O_3 to I^- along with the physical processes that control O_3 dry deposition has been shown to improve model comparisons to observations of both oceanic dry deposition velocity and remote marine surface O_3 concentrations (Luhar et al., 2017, 2018; Pound et al., 2020).

Photochemical cycling of iodine in the atmosphere leads to efficient chemical loss of O_3. Iodine compounds photolyze to produce atomic iodine (I) which is then rapidly oxidised by O_3 to form iodine oxide (IO). The dominant loss route is IO + HO_2 to return to HOI, which on photolysis leads to net loss of O_3 (Sommariva et al., 2012). The inclusion of iodine emissions and subsequent chemistry into global chemistry transport models decreases tropospheric ozone concentration by 6-10% (Sherwen et al., 2016; Iglesias-Suarez et al., 2020; Pound et al., 2023c) with the largest impact being in the marine boundary layer (MBL) and coastal regions. IO can also impact both HO_x (OH + HO_2) and NO_x (NO + NO_2) concentrations (Sommariva et al., 2012; Sherwen et al., 2016). However, globally, iodine has a small impact on the atmospheric OH concentration. Whilst the reduction in O_3 by iodine reduces the primary chemical production of OH, iodine chemistry increases the conversion of HO_2 to OH, offsetting the reduction in primary production (Sherwen et al., 2016; Pound et al., 2023c).

Organic iodine species have been shown in laboratory experiments as the source of nucleation of new particles in coastal environments (Hoffmann et al., 2001). Recent work has also supports atmospheric iodine playing an important role in partial formation in the MBL, with the impact of iodine on aerosol formation and growth larger than previously thought (Huang et al., 2022). Combined with more efficient recycling of iodine from aerosol particles Tham et al. (2021), this could mean that current global chemistry transport models underestimate the role of iodine in aerosol formation and its spatial range of impact.

Recent observations show that approximately 0.7 ppt of reactive iodine species are injected into the stratosphere (Koenig et al., 2020). This has an important impact on stratospheric O_3, particularly in the tropical lower stratosphere (Saiz-Lopez et al., 2015). Based on these iodine levels reaching the stratosphere, recent model studies have shown that iodine can significantly impact the Antarctic O_3 hole, with iodine's role in modulating stratospheric O_3 likely to increase in relative importance as anthropogenic chlorine and bromine emissions decrease (Cuevas et al., 2022).

I^- in the ocean is formed from the thermodynamically more stable iodate (IO_3^-) via biological reduction processes (Truesdale and Jones, 2000; Chance et al., 2007; Amachi, 2008; Wadley et al., 2020). I^- and IO_3^- combined represent the majority of the total iodine in the ocean. Due to the dependence on biological reduction, I^- concentrations in the ocean could display sensitivity to both seasonal and climate timescales (Carpenter et al., 2021).

Following this initial reaction of O_3 + I^-, further aqueous chemistry in the ocean surface microlayer (SML) produces iodinated compounds which can subsequently be emitted into the atmosphere. The largest components of iodine emissions from the ocean surface are the inorganic compounds HOI and I_2, which are thought to contribute approximately 2 Tg yr^{-1} of iodine to the global atmosphere (Carpenter et al., 2021). An additional 0.6 Tg yr^{-1} of iodine arises from the emission of iodinated

https://doi.org/10.5194/egusphere-2023-2447
Preprint. Discussion started: 17 November 2023

hydrocarbons (CH_3I, CH_2I_2, CH_2IBr and CH_2ICl) (Jones et al., 2010; MacDonald et al., 2014; Prados-Roman et al., 2015).

The O_3 uptake rate by aqueous iodide solutions has been found to be significantly decreased by the addition of surfactants which form a monolayer across the solution and suppress exchange (Rouvière and Ammann, 2010). The addition of organic material has also been found to suppress I_2 emissions from I^- solutions, with this largely being attributed to a decrease in the net transfer of I_2 from the aqueous to gas phase (Reeser and Donaldson, 2011; Shaw and Carpenter, 2013; Tinel et al., 2020).

Anthropogenic activity has contributed to increased iodine emissions since preindustrial times (Cuevas et al., 2018; Legrand et al., 2018), largely due to increased tropospheric O_3 increasing inorganic iodine emissions from the ocean. The increase in anthropogenic emissions from preindustrial to the present day has also shifted the partitioning of inorganic halogens from reactive to reservoir species (Barrera et al., 2023). Model studies using future climate scenarios forecast a key role of iodine in O_3 destruction through the 21st century (Badia et al., 2021).

Carpenter et al. (2013) created a kinetic box model of the SML to predict inorganic iodine emissions which were parameterised as functions of surface O_3 concentration, I^- concentration in the ocean and wind speed. This model predicts exponentially increasing inorganic iodine emissions as wind speed decreases due to an increasing fraction of iodine being emitted to the atmosphere as opposed to being mixed with the underlying water. As such, a minimum wind speed of 5.5 ms^{-1} was applied when implemented in the global chemistry transport model GEOS-Chem (Sherwen et al., 2016). This SML model also does not directly couple the SML chemistry to O_3 dry deposition and as such is unable to capture feedback between O_3 deposition, I^- depletion in the SML (Schneider et al., 2020), and the chemical production and emission of inorganic iodine compounds. Finally, the equations provided by Carpenter et al. (2013) did not include a temperature dependence. In reality, there are a host of temperature-dependent processes involved in iodine emissions including the O_3+I^- reaction (Brown et al., 2023), the diffusivity of O_3 (Johnson and Davis, 1996) and the solubility of HOI and I_2.

Several experiments have measured the rate constant of the O_3 + I^- reaction at a single temperature (Garland et al., 1980; Hu et al., 1995; Liu et al., 2001). A temperature-dependent rate by Magi et al. (1997) has been used in previous work to model oceanic O_3 dry deposition (Luhar et al., 2017, 2018; Pound et al., 2020) and inorganic iodine emissions (Carpenter et al., 2013). However, the Magi et al. (1997) laboratory study used iodide concentrations of 0.5-3.0 M, which are substantially higher than the typical ocean surface range of 10-100 of nM (Chance et al., 2014). At I^- concentrations above 1000 nM, the reaction between O_3 and I^- occurs at the water surface (Moreno et al., 2018). However, with environmental concentrations of I^-, 10-100 nM, the reaction mainly occurs by a different mechanism, within the bulk aqueous phase (Moreno et al., 2018). Ozone uptake experiments under environmentally comparable I^- concentrations also support the aqueous reaction dominating the O_3 + I^- reaction (Schneider et al., 2020; Brown et al., 2023). Recently, Brown et al. (2023) have calculated a new temperature-dependent rate for O_3 + I^- under environmentally comparable iodide concentrations (100-10000 nM) and an O_3 mixing ratio of 40 ppb at 1 atm. A range of temperatures from 288-303 K were applied, yielding a temperature dependence

https://doi.org/10.5194/egusphere-2023-2447
Preprint. Discussion started: 17 November 2023

which can be applied to the interaction of ozone and iodide in the ocean surface. This rate is comparable to other experimental results which did not sample a range of temperatures (Garland et al., 1980; Liu et al., 2001; Hu et al., 1995).

Here we propose a new air-SML-ocean exchange model to couple the processes of oceanic ozone dry deposition to inorganic iodine emissions, which incorporates recent advancements in inorganic iodine chemistry. Section 2 describes the construction of the model and the equations used to describe the physical and chemical components. Sections 3 to 5 diagnose the model's sensitivity to mixing, rate of $O_3 + I^-$ reaction, and salinity and inter-halogen reactions. We then compare this new model to the existing model from Carpenter et al. (2013) (section 6) and experimental results (section 7). Finally, parameterised functions for estimating HOI and I_2 emissions calculated by this coupled ocean-atmosphere exchange model (section 8) are implemented in a global chemical transport model (GEOS-Chem Classic) to give a new estimate for global inorganic iodine emissions and their impact on tropospheric O_3 (section 9).

2 SML box model description

Figure 1 shows a simplified overview of the ocean-atmosphere exchange model described in this paper. Ozone deposition is based on the resistance-in-series scheme and is further described in section 2.1. The chemistry scheme employed is described in section 2.2. Finally, the mixing of the SML with the atmosphere and the ocean is based on the method described by Cen-Lin and Tzung-May (2013) which is described in sections 2.3.1 and 2.3.2 respectively. Table 1 lists all the inputs, outputs and variables used to calculate the flux of ozone into the SML and the emission of inorganic halogens from the SML.

The model was developed in Python using Cantera as the chemistry solver (Goodwin et al., 2022). The model presented here also uses functions from SciPy (Virtanen et al., 2020), Pandas (development team, 2020), and NumPy (Harris et al., 2020). Calculations of the salinity and temperature-dependent unitless Henry's law (H), Schmidt number in the air (S_{ca}) and water (S_{cw}), airside (k_a) and waterside (k_w) transfer velocities are calculated using the recommended functions from Johnson (2010). The model runs presented here used a physical timestep of 1×10^{-4} s.

2.1 Coupled ozone dry deposition

Ozone dry deposition velocity (v_d) is calculated using the resistance-in-series scheme based on Wesely and Hicks (1977), equation 1, this is then used to calculate the flux of ozone into the ocean surface microlayer. Airside resistances that represent turbulent transport to the surface (r_a) and transport through the atmospheric quasilaminar sub-layer, which is the air directly above the surface microlayer (r_b), are calculated using equations 2 and 3 respectively (Chang et al., 2004).

https://doi.org/10.5194/egusphere-2023-2447
Preprint. Discussion started: 17 November 2023

$$v_d = \frac{1}{r_a + r_b + r_c} \tag{1}$$

$$r_a = \frac{u_{10}}{u^{*2}} \tag{2}$$

$$r_b = \frac{5}{u^*} S_{ca}^{2/3} \tag{3}$$

Where u is the 10m wind speed with units of ms^{-1}, u^* is the friction velocity with units of ms^{-1}, and S_{ca} is the Schmidt number of O_3 in air and is calculated using the method from Tsilingiris (2008) as recommended by Johnson (2010).

The surface resistance (r_c) captures the chemical and physical processes in the SML which control ozone loss. We employ the two-layer method of Luhar et al. (2018) to calculate r_c which is shown in equation 4.

$$r_c = \frac{1}{\alpha\sqrt{aD}} \left[\frac{\Psi K_1(\xi_\delta)\sinh(\lambda) + K_0(\xi_\delta)\cosh(\lambda)}{\Psi K_1(\xi_\delta)\cosh(\lambda) + K_0(\xi_\delta)\sinh(\lambda)} \right] \tag{4}$$

with,

$$\xi_\delta = \left[\frac{4a}{\kappa u_w^*} \left(\delta_m + \frac{D}{\kappa u_w^*} \right) \right]^{\frac{1}{2}} \tag{5}$$

$$\Psi = \left[1 + \left(\frac{\kappa u_w^* \delta_m}{D} \right) \right]^{\frac{1}{2}} \tag{6}$$

and

$$\lambda = \delta_m \sqrt{\frac{a}{D}} \tag{7}$$

Where κ is the von Kármán constant (≈ 0.4), α is the dimensionless solubility of O_3 from Morris (1988),

$$\alpha = 10^{-0.25-0.013(T-273.16)} \tag{8}$$

The chemical reactivity is given by $a = k[I^-]$, where the second order rate-coefficient (k) is given by either Magi et al. (1997) or Brown et al. (2023) with units of $\mathrm{M}^{-1}\mathrm{s}^{-1}$.

The diffusivity in water (D, $\mathrm{m}^2\mathrm{s}^{-1}$) is from Johnson and Davis (1996) and given by

$$D = 1.1 \times 10^{-6} exp\left(\frac{-1896}{T} \right) \tag{9}$$

https://doi.org/10.5194/egusphere-2023-2447
Preprint. Discussion started: 17 November 2023

u_w^* (ms^{-1} is the water-side friction velocity, δ_m is the thickness of the reaction-diffusion layer of the sea-surface microlayer (m) calculated using 10 (Luhar et al., 2017). K_0 and K_1 are modified Bessel functions of the second kind with order zero and one respectively.

$$\delta_m = \sqrt{\frac{D}{a}} \tag{10}$$

The dry deposition velocity (v_d) is coupled to the SML chemistry via the I^- concentration and is recalculated as the model advances in time.

2.2 Chemistry

The aqueous inorganic halogen chemistry scheme used in this model is shown in Table 2. Here we employ an extended version of the iodine chemistry scheme used by Carpenter et al. (2013) and similar to that of Schneider et al. (2023) with the addition of further inter-halogen reactions involving bromine and chlorine species. A further difference between this chemistry scheme and that of Carpenter et al. (2021) is that we explicitly include the reaction step of O_3 + I^- producing IO^- (R1a) rather than HOI directly, alongside its subsequent conversion to HOI (R7). This has little impact on the total simulated inorganic iodine emissions as IO^- quickly reacts to form HOI at ocean pH, but presents a more complete representation of the chemistry.

To explore the sensitivity of total iodine emissions to the rate coefficient of the O_3 + I^- reaction, two different forms of the temperature-dependent rate coefficient are used. The first of these (reaction R1a from table 2) uses the rate published by Magi et al. (1997) which is also the rate used by Carpenter et al. (2013) in their model. The second rate (reaction R1b from table 2) is the more recent temperature-dependent rate from Brown et al. (2023) which has a much weaker temperature dependence than that of Magi et al. (1997). The different temperature dependencies of these two rates are shown in figure 2.

2.3 Mixing processes

2.3.1 Emissions of inorganic iodine

The net flux of a species from the SML into the atmosphere (F_a) is calculated from the concentration in the SML (C_{sml}) and the concentration in the atmosphere (C_a, equation 11). Atmospheric fluxes are calculated for HOI, I_2, IBr and ICl, HOCl, HOBr, Br_2, Cl_2, BrCl. HOI and I_2 have the largest fluxes, with the other species emitted in negligible amounts due to their high solubility and relatively low concentrations in the SML.

$$F_a = k_a(H * C_{sml} - C_a) \tag{11}$$

https://doi.org/10.5194/egusphere-2023-2447
Preprint. Discussion started: 17 November 2023

k_a is calculated following the recommendation from Johnson (2010) using equation 12

$$k_a = + \frac{u_*}{13.3 S_{ca}^{0.5} + C_D^{-0.5} - 5 + \frac{ln(S_{ca})}{2\kappa}} \tag{12}$$

where u_* is the friction velocity (ms^{-1}), C_D is the drag coefficient (ms^{-1}) from Smith (1980)

$$10^3 C_D = 0.61 + 0.063 u_{10} \tag{13}$$

2.3.2 Ocean mixing with SML

This model employs SML concentrations mixing with the bulk ocean concentration (C_b) on two timescales and follows the approach used by Cen-Lin and Tzung-May (2013). The first mixing process, molecular transfer, occurs on the order of 0.1 - 1 seconds and is given by equation 14.

$$F_b = R k_w (C_b - C_{sml}) \tag{14}$$

where R accounts for the effects of surfactants suppressing the transport between the SML and bulk ocean. A value of 0.9 is used in this study to represent the open ocean (GOL, 1988; Frew et al., 1990; Cen-Lin and Tzung-May, 2013). k_w is calculated using equation 15 which follows the recommendations of Johnson (2010) in using the Nightingale et al. (2000) approach. u_{10} is the 10m wind speed, S_{cw} is the Schmidt number of the gas in water and S_{c600} Schmidt number of CO_2 at 20 °C.

$$k_w = (0.222 u_{10}^2 + 0.333 u_{10}) (\frac{S_{cw}}{S_{c600}})^{0.5} \tag{15}$$

The second mixing process is surface renewal, representative of larger scale eddy mixing, and is given by equation 16. It is a significantly slower process than the mixing described above and is typically of the order of minutes or longer, but has been included for completeness. Surface renewal and the suppression of transfer velocity by surfactants (R) are new developments in this model compared to Carpenter et al. (2013).

$$F_r = (3.42 \times 10^{-3} u_{10} + 2.7 \times 10^{-3})(C_b - C_{sml}) \tag{16}$$

Fluxes for mixing between the SML and bulk ocean are calculated for HOI, I_2, O_3, IBr, ICl, IO_3^-, HOBr, HOCl, Br_2, Cl_2, BrCl, I^-, Br^- and Cl^-. The mixing processes described here are only representative of passive diffusion and do not take into account any electrostatic effects. Solutions with ions have been found to have stronger electric fields at the air-water interface than within the bulk due to charge separation and this can contribute to an increased concentration of ions and enhanced reaction rates (Xiong et al., 2020; Hao et al., 2022). However, given that the fast turbulent-driven mixing of the SML with the bulk water and the chemical depletion of I^- within the SML occur on timescales of seconds or less under typical conditions, we consider additional effects which could impact the enhancement or depletion of I^- within the SML are likely secondary. The

https://doi.org/10.5194/egusphere-2023-2447
Preprint. Discussion started: 17 November 2023

control of I− in the SML by the equilibrium of chemical and physical processes represents a significant difference between this work and that of Carpenter et al. (2013), where it was prescribed as a constant. The impact of this difference is explored in section 3.

The concentration of I^- is set based on the conditions being studied by the model, unless otherwise stated the sensitivity studies presented here use a concentration of 100nM. Br^- concentrations are set at 0.86 mM and Cl^- at 0.55 M to replicate typical ocean salinity. The oceanic concentration of IO_3^- is set at 200 nM (Chance et al., 2020). All other species are assumed to have zero bulk oceanic concentrations. H^+ and OH^- are not subject to mixing and are manually set at each time-step to maintain a constant pH of 8.

3 Depletion of SML iodide

One difference between this and previous work is the model prediction of depletion of I^- in the SML at low wind speeds (figures 3 and 4) due to its reaction with O_3. This is a direct consequence of the slow replenishment of I^- in the SML from mixing with bulk water rather than being a fixed quantity as in previous models. Depletion of I^- has been previously detected experimentally in artificial seawater (Schneider et al., 2023). The effect of this depletion on total inorganic iodine emission and the composition of that emission is shown in figure 3. To a lesser extent, depletion of I^- is also greater at higher SST, as shown in figure 4; this is entirely driven by the temperature dependence of the O_3 + I^- reaction.

The depletion of I^- accounts for roughly an 11% reduction in total inorganic iodine emissions at 2 ms^{-1} wind speed, 285 K, 30 ppb O_3, and 100 nM of I^- in bulk water (figure 3). The reduction in SML I^- concentration also reduces O_3 dry deposition velocity by 15% under the same conditions.

4 Sensitivity to the temperature dependence of the I^- + O_3 reaction

Here we compare two temperature-dependent rate constants for the I^- + O_3 reaction. The first of these is that of Magi et al. (1997), which has been used in the previous model of Carpenter et al. (2013). We compare this to the more recent rate from Brown et al. (2023) which was derived from experiments conducted at I^- concentrations of ∼100 - 10000 nM. The difference in the temperature dependence of total inorganic iodine emission is shown in figure 5. The newer rate constant results in substantially higher total inorganic iodine emissions at low SST. At 285K, total inorganic iodine emissions increase by ∼170% when using the rate coefficient from Brown et al. (2023) compared to Magi et al. (1997) (Figure 5a), and O_3 dry deposition velocity increases by 36%. Both increases are offset by I^- enrichment decreasing from ∼95% to ∼87% at the same temperature (Figure 5c). Increased depletion of I^- in the SML also results in the production pathways of I_2 from HOI becoming

https://doi.org/10.5194/egusphere-2023-2447
Preprint. Discussion started: 17 November 2023

less competitive, resulting in the amount of I_2 emission relative to HOI decreasing (Figure 5b). At higher temperatures (above ~25°C, figure 2), the Brown et al. (2023) rate is slower than that of Magi et al. (1997), resulting in decreased HOI production and lower overall emissions. All subsequent experiments using the box model use the Brown et al. (2023) rate due to it better reflecting the O_3+I^- reaction under oceanic conditions.

5 I_2 emission salinity sensitivity

The experimental work of MacDonald et al. (2014) found a strong increase in I_2 emission at higher salinity, which was replicated in their accompanying model results. We also predict a positive salinity dependence on I_2 emissions in our base model (figure 6). The increase in I_2 emissions is partly from the additional chemical pathway to produce I_2 via ICl as concluded by MacDonald et al. (2014) (reactions R13, R15 and R17 in table 2). Additionally, the changes in solubility (due to salinity due to the salinity dependence of H and S_{cw}, salting out effect), increase the total iodine emissions, shown by the difference in green and yellow lines in figure 6 where the chloride concentration was set to achieve a salinity of 35 PSU but the chlorine chemistry was removed from the chemical mechanism. The increase in total iodine emissions from the increase in I_2 emission has a negligible impact on HOI emissions, as HOI is in excess in the SML (Carpenter et al., 2013).

The largest increase in I_2 emission with the addition of salinity is observed in low turbulence conditions (low wind speed, figure 6b); here the effects on solubility have a larger effect than the additional chemical pathway to I_2 production provided by Cl^-. Under the conditions used in this study, I_2 emissions are increased by ~150% with the addition of Cl^-. However, this is less than the 250% increase observed by MacDonald et al. (2014). Differences between experimental results and this model are discussed further in section 7. Figure 6 shows that similar to chloride, increasing bromide increases total I_2 production. This increase is the result of the additional pathway via IBr to produce I_2 (reactions R12 and R14 in table 2).

In contrast to these results, more recent work from Tinel et al. (2020) and Schneider et al. (2023) did not find an increase in I_2 emissions from increasing Cl^-, instead, I_2 emissions were suppressed in saline samples compared to just iodide solutions. Schneider et al. (2023) found that their results could be replicated by shifting the equilibrium for reaction R15a in table 2 to favour I_2Cl^- over I_2 (reaction R15b in table 2). The result of implementing that change to the equilibrium in this model is shown in figure 7; the rate of I_2 production through the additional chemical pathway provided by ICl is reduced and iodine emissions decrease by up to 5%. Depletion of I^- is unaffected.

https://doi.org/10.5194/egusphere-2023-2447
Preprint. Discussion started: 17 November 2023

6 Comparisons to existing model

Figure 8 compares the total iodine emissions predicted in this work to that of Carpenter et al. (2013) across wind speed, iodide, ozone and temperature ranges. The new model uses the $O_3 + I^-$ rate from Brown et al. (2023) and the updated equilibrium of reaction R15b from Schneider et al. (2023). Temperature dependence was not included in the Carpenter et al. (2013) equations. Two versions of the Carpenter et al. (2013) model are used in the wind speed comparison. The first is the equations as presented (solid black line), the second has a minimum wind speed of 5.5 ms^{-1} applied (dashed black line, as used in the global modelling study of Sherwen et al. (2016)). For total iodine emission at the highest wind speeds, the new model tends towards the old model. This is due to the efficient mixing at these higher wind speeds resulting in negligible I^- depletion in the SML, thus more closely resembling the old model which included a constant I^- concentration in the SML. As wind speed decreases, the two models diverge in their prediction of total iodine emission with the new model predicting less emission flux than the capped and uncapped (Carpenter et al., 2013) model. This decrease is most notable at very low wind speeds where the new model tends towards no iodine emission as wind speed tends towards zero, rather than the Carpenter et al. (2013) model where total iodine emissions exponentially increase as wind speed tends to zero.

Carpenter et al. (2013) found a simple multiplicative and approximately linear relationship between O_3 concentration and total iodine emission. The slightly dampened relationship between O_3 and total iodine emission in this model is likely because higher O_3 concentration causes a greater depleting effect on SML I^- concentration, reducing total iodine emission. The new model predicts a similar trend of I^- dependence of total iodine emission to Carpenter et al. (2013). Additionally, the new model predicts that I_2 contributes a larger percentage of total iodine emissions, despite the change made to the chemistry scheme to reflect lower I_2 emissions under oceanic salinity. This difference is likely due to a reduced HOI emission flux from the SML, resulting in more of the aqueous HOI remaining in the SML which can subsequently produce more I_2.

7 Comparisons to experimental data

Table 3 compares published experimental results for I_2 fluxes to predictions from this model under conditions that match those used in the various experimental studies. One limitation in this comparison is replicating the waterside turbulence due to stirring (or not) of the aqueous solution and from the gas flow over the solution. Experimental setups which do not stir the solution have very different dynamics to the ocean surface, which this model has been designed to replicate. Additionally, some experimental results use O_3 and I^- concentrations significantly higher than typical environmental conditions due to measurement instrument sensitivity (table 3). The model significantly underestimates experimental results where the solutions were not stirred, possibly due to a high depletion of surface iodide under such conditions which reduces the potential for gaseous iodine emissions (Schneider et al., 2023). For stirred experiments however, the model predicts a similar range of I_2 emissions as the experiments.

https://doi.org/10.5194/egusphere-2023-2447
Preprint. Discussion started: 17 November 2023

8 Parameterised equation for HOI and I_2 emission flux

Here we present two mathematical functions to predict HOI (equation 17) and I_2 (equation 18) emission fluxes based on [O_3], bulk [I^-], wind speed and SST. A non-linear least squares fit was used on 5000 unique combinations of model inputs covering environmentally comparable ranges of each variable (5-60 ppb of O_3, 0.1-11.1 ms-1 wind speed, 20-240 nM bulk [I^-] and 274-300 K SST). All other parameters are kept constant in the sensitivity analysis. The model sensitivity studies are run using the O_3 + I^- rate from Brown et al. (2023) and the updated equilibrium of reaction R15b from Schneider et al. (2023). These equations have a high correlation with the results from the SML box model, R^2 = 0.90 for HOI and R^2 = 0.84 for I_2, and no strong bias in over or underestimating the model results (figure 9).

$$HOI = 6.1 \times 10^{-15} \, (u + 1.1) \, e^{-0.05T - \frac{(u+2.1)^2}{22}} [O_3]_g^{0.93} [I^-]^{0.63} \tag{17}$$

$$I_2 = 1.4 \times 10^{-17} \, (1.1u + 3) \, e^{-0.01T - \frac{(u+3.6)^2}{33}} [O_3]_g^{0.8} [I^-]^{1.5} \tag{18}$$

where HOI and I_2 emission are in kg m^{-2} s^{-1}, T is the sea surface temperature (°C), u is the 10 m wind speed (ms^{-1}), $[I^-]$ is the bulk water iodide concentration (nM), and $[O_3]_g$ is the atmospheric ozone mixing ratio (ppb).

The most notable difference between the parameterised equations presented here and those from Carpenter et al. (2013) is the inclusion of T as a parameter. Carpenter et al. (2013) found a linear relationship between both HOI and I_2 emissions and atmospheric O_3. This relationship with O_3 is reduced for HOI which can be attributed to the impact of I^- depletion in the SML being increased at higher O_3 concentrations, reducing the rate at which the O_3 + I^- reaction can occur. The effect of O_3 concentration on I^- depletion is further enhanced for I_2 production (hence a further reduction in the I_2 dependence on O_3 concentration) as the subsequent chemical pathways to convert HOI to I_2 also depend on the availability of I^- in the SML. I^- depletion can also explain the increase in dependence of HOI emission on SML [I^-] (from a power of 0.5 to 0.63) and I_2 (from a power of 1.3 to 1.5) due to a relative increase in the availability of I^- in the SML at higher bulk water concentrations.

9 Implementing the new iodine emission equations in GEOS-Chem Classic

We use the GEOS-Chem classic model (Bey et al., 2001) version 14.1.1 (GCC14.1.1, 2023) for global modelling of inorganic iodine emissions and their impact on tropospheric composition. GEOS-Chem Classic is a chemical transport model with a HOx-NOx-VOC-O_3-halogen-aerosol tropospheric chemistry scheme. The current version of the halogen chemistry scheme is described by Wang et al. (2021), with organic iodine emissions based on Ordóñez et al. (2012), and inorganic iodine emissions based on Carpenter et al. (2013) (as implemented by Sherwen et al. (2016)). The current inorganic iodine emissions in GEOS-Chem use surface oceanic iodide concentrations based on MacDonald et al. (2014), which under-predicts compared to observations (Sherwen et al., 2019) and differs from the iodide field used in calculating O_3 dry deposition which uses Sherwen

https://doi.org/10.5194/egusphere-2023-2447
Preprint. Discussion started: 17 November 2023

et al. (2019) (Pound et al., 2020). Here, we use the most up-to-date, machine learning-derived, iodide field from Sherwen et al. (2019) for both inorganic iodine emissions and O_3 dry deposition.

A global spatial resolution of 4°x5° on the standard vertical grid (72 vertical levels) is used, running with chemistry in both the troposphere and stratosphere. Meteorological data is from MERRA-2 (Gelaro et al., 2017). Two model runs were conducted which were identical in configuration, apart from inorganic iodine emissions. The first uses the default inorganic iodine emissions based on the equations from Carpenter et al. (2013) driven by MacDonald et al. (2014) oceanic I^-, and the second of the two runs using the new iodine emission equations presented in this work (equations 17 and 18) driven by Sherwen et al. (2019) oceanic I^-. All other emission and time-step configurations were left at their recommended settings. Model simulations were conducted from the 1^{st} of July 2019 to the 1^{st} of July 2021, with the first year of the simulation considered a "spin-up" to allow the model to reach equilibrium.

The new parameterizations increase the total global inorganic iodine emissions from 2.84 Tg yr^{-1} to 2.95 Tg yr^{-1}, an increase of 3.7%. Additionally, there is a slight increase in the ratio of I_2 emissions compared to HOI, with I_2 now accounting for 6.2% (previously 5.7%), however, this difference would not change the impact of iodine on the troposphere as both HOI and I_2 rapidly photolyse. Whilst this is a relatively small global total change, there is a significant re-distribution of total iodine emissions, with emissions from equatorial waters decreasing and high latitude emissions increasing, as shown in figure 10.

The change in the distribution of inorganic iodine emissions substantially increases high latitude IO (and IO_x) concentrations, with percentage changes of >1000% as the base case model predicts very low or no IO concentration in these regions (figure 11). Equatorial IO is decreased, mirroring the drop in inorganic iodine emissions from warm waters. However, despite large regional changes, the change in area-weighted mean vertical iodine speciation is minimal. Figure 12 compares published observations of average daytime surface IO mixing ratios to equivalent model predictions. The change in iodine emissions has little effect on the average model root mean square error, increasing it from 0.48 to 0.51 ppt. Wang et al. (2021) found less disagreement between their model and observation comparisons, however, that study included sea salt debromination which has a large impact on tropospheric O_3 and is by default deactivated in version 14.1.1 of GEOS-Chem. The increase in high latitude oceanic emissions of HOI and I_2 reduces the model error at the two Antarctic locations (Bharati and Maitri bases) included in figure 12, however the model still significantly underestimates IO levels in this region. Atmospheric iodine observations made in the Antarctic region have been shown to have a source from sea ice (Saiz-Lopez et al., 2007; Atkinson et al., 2012); and a direct source of atmospheric IO from the snowpack (Frieß et al., 2010), these processes are not currently represented in the model.

As the total iodine and global average speciation change only negligibly with the new parameterisation, there is a similarly negligible change in the tropospheric O_3 burden (from 329.7 Tg to 330.3 Tg, an increase of 0.2%). However, as with IO, there are larger regional changes in both surface and zonal O_3, as shown in figure 13. Tropospheric O_3 at higher latitudes is decreased with the largest absolute and percentage changes above the Southern Ocean, while O_3 above the equator and tropics increases.

https://doi.org/10.5194/egusphere-2023-2447
Preprint. Discussion started: 17 November 2023

The largest absolute and percentage change is above the Indian Ocean.

Figure 14 shows the impact of the change in iodine emissions on surface ozone predictions. For this, we compare the model to a selection of surface ozone measurements from several World Meteorological Organization (WMO) Global Atmosphere Watch sites around the world (GAW; http://www.wmo.int/pages/prog/arep/gaw/gaw_home_en.html, accessed through EBAS http://ebas.nilu.no/, the database infrastructure operated by NILU – Norwegian Institute for Air Research).

At the northern high latitudes, we compare to O_3 observations made in Greenland (panel a of figure 14). The model disagreement at this site, measured using root mean square error (RMSE), decreases from 3.7 ppbv to 3.5 ppbv (5%), however, the model remains unable to replicate springtime O_3 depletion events that occur in the high latitudes.

Mace Head, Ireland (panel b of figure 14) observes air masses that inflow into Europe from the North Atlantic. The model predictions remain within the observed range, however, monthly mean RMSE increases by 21% (from 3.9 ppbv to 4.7 ppbv). Model error in surface O_3 at remote tropical locations, such as Cape Verde Atmospheric Observatory (CVAO) in Cabo Verde (panel b of figure 14), is generally low (2.2 ppbv). The decrease in inorganic iodine emissions from the ocean surrounding these islands marginally increases this error (2.4 ppbv, +10%), however, like Mace Head, the model remains within the observed range.

Comparisons between GEOS-Chem and O_3 observations in the Antarctic and Southern Ocean have consistently shown a low bias in the model (Young et al., 2013; Sherwen et al., 2016; Schmidt et al., 2016; Pound et al., 2020). As with northern high latitudes, the model is also unable to replicate halogen-driven O_3 depletion events which occur during Antarctic spring. The decrease in surface O_3 concentrations over the Southern Ocean and Antarctic caused by the increase in Southern Ocean inorganic iodine emissions exacerbates the underestimate of O_3 observations made at Neumayer and Cape Grim (panels d and f of figure 14), increasing RMSE by 44% (from 4.5 ppbv to 6.5 ppbv) and 50% (from 1.8 ppbv to 2.7 ppbv) respectively. This trend does not apply to the Southern hemisphere location of Ushaia (panel e of figure 14), which has a small decrease in model error (4%, from 2.4 ppbv to 2.3 ppbv).

There is negligible change in area-weighted mean tropospheric OH concentration and tropospheric CH_4 lifetime (both <0.1%).

10 Conclusions

Here we present a new SML box model that incorporates recent advancements in inorganic iodine chemistry, O_3 deposition velocity calculation and improvements to the representation of surface ocean mixing. One key difference between this and previous work is the simulation of depletion of I^- in the SML, which is dependent on the turbulence and the O_3 concentration

https://doi.org/10.5194/egusphere-2023-2447
Preprint. Discussion started: 17 November 2023

and has been previously observed in experiments using artificial seawater. This results in a dampening of iodine emissions in low wind speed conditions.

From this new box model, we derive parameterised equations for HOI and I_2 emissions which can then be implemented in global models. Using these updated equations in GEOS-Chem results in only a small change in total global inorganic iodine emissions (+3.7%) and a negligible change to tropospheric O_3 burden (+0.2%). However, it does result in reduced inorganic iodine emissions in equatorial waters and increased emissions from high-latitude waters.

There are still a number of uncertainties that remain in oceanic iodine chemistry and the emissions of iodine from the SML that have not been addressed by this work. In particular, the model does not account for organic-iodine or organic-ozone interactions in the SML or surfactants suppressing ocean-atmosphere exchange. These processes are not sufficiently well understood to include in models but should be a focus of future work.

Code availability. GEOS-Chem source code is openly available on GitHub (https://github.com/geoschem/geos-chem). This work used model version 14.1.1 (GCC14.1.1, 2023).

The box model developed here has been made publicly available on GitHub (https://github.com/r-pound/COAGEM) as version 1.0.0 (Pound et al., 2023a)

Data availability. The complete results for sensitivity runs used to produce the parameterised HOI and I_2 have been archived and are openly available (Pound et al., 2023b)

Author contributions. R.J.P performed model development, conducted the simulations and analysed the output. L.V.B contributed to model development and analysis. M.J.E., L.J.C. and R.J.P developed the project. All authors contributed to the writing of this manuscript

Competing interests. The authors declare that they have no conflict of interest.

Acknowledgements. We thank WMO GAW and the individual sites that make up this network, for the availability of the surface ozone data through EBAS, managed by the Norwegian Institute for Air Research.

This project was undertaken on the Viking Cluster, which is a high performance compute facility provided by the University of York. We are grateful for computational support from the University of York High Performance Computing service, Viking and the Research Computing team.

L.J.C, R.J.P and L.V.B acknowledge funding from the European Research Council (ERC) under the European Union's Horizon 2020 programme (Grant agreement No. 833290).

https://doi.org/10.5194/egusphere-2023-2447
Preprint. Discussion started: 17 November 2023

MJE thanks the UK National Centre for Atmospheric Science for funding.

We thank the GEOS-Chem community for developing the model over the past decades.

https://doi.org/10.5194/egusphere-2023-2447
Preprint. Discussion started: 17 November 2023

References

Surfactant effects on air-sea gas exchange under turbulent conditions, Deep Sea Research Part A. Oceanographic Research Papers, 35, 1953–1970, https://doi.org/https://doi.org/10.1016/0198-0149(88)90119-7, 1988.

Amachi, S.: Microbial Contribution to Global Iodine Cycling: Volatilization, Accumulation, Reduction, Oxidation, and Sorption of Iodine, Microbes and Environments, 23, 269–276, https://doi.org/10.1264/jsme2.ME08548, 2008.

Atkinson, H. M., Huang, R.-J., Chance, R., Roscoe, H. K., Hughes, C., Davison, B., Schönhardt, A., Mahajan, A. S., Saiz-Lopez, A., Hoffmann, T., and Liss, P. S.: Iodine emissions from the sea ice of the Weddell Sea, Atmospheric Chemistry and Physics, 12, 11 229–11 244, https://doi.org/10.5194/acp-12-11229-2012, 2012.

Badia, A., Iglesias-Suarez, F., Fernandez, R. P., Cuevas, C. A., Kinnison, D. E., Lamarque, J.-F., Griffiths, P. T., Tarasick, D. W., Liu, J., and Saiz-Lopez, A.: The Role of Natural Halogens in Global Tropospheric Ozone Chemistry and Budget Under Different 21st Century Climate Scenarios, Journal of Geophysical Research: Atmospheres, 126, e2021JD034 859, https://doi.org/https://doi.org/10.1029/2021JD034859, 2021.

Barrera, J., Kinnison, D., Fernandez, R., Lamarque, J., Cuevas, C., Tilmes, S., and Saiz-Lopez, A.: Comparing the Effect of Anthropogenically Amplified Halogen Natural Emissions on Tropospheric Ozone Chemistry Between Pre-Industrial and Present-Day, Journal of Geophysical Research: Atmospheres, 128, https://doi.org/10.1029/2022JD038283, 2023.

Beckwith, R. C., Wang, T. X., and Margerum, D. W.: Equilibrium and kinetics of bromine hydrolysis, Inorg. Chem., 35, 995– 1000, 1996.

Bey, I., Jacob, D. J., Yantosca, R. M., Logan, J. A., Field, B. D., Fiore, A. M., Li, Q., Liu, H. Y., Mickley, L. J., and Schultz, M. G.: Global modeling of tropospheric chemistry with assimilated meteorology: Model description and evaluation, J GEOPHYS RES-ATMOS, 106, 23 073–23 095, https://doi.org/10.1029/2001JD000807, 2001.

Bichsel, Y. and von Gunten, U.: Hypoiodous acid: kinetics of the buffer-catalyzed disproportionation, Water Research, 34, 3197–3203, https://doi.org/https://doi.org/10.1016/S0043-1354(00)00077-4, 2000.

Brown, L. v., Ives, L., Pound, R. J., Jones, M., Andrews, S., and Carpenter, L. J.: Temperature Dependence of the Ozone Iodide Reaction and Implication for Oceanic Emissions of Iodine, Pending Submission, X, X, https://doi.org/X, 2023.

Carpenter, L., Chance, R. J., Sherwen, T., Adams, T. J., Ball, S. M., Evans, M. J., Hepach, H., Hollis, L. D. J., Hughes, C., Jickells, T. D., Mahajan, A., Stevens, D. P., Tinel, L., and Wadley, M. R.: Marine iodine emissions in a changing world, Proceedings of the Royal Society A: Mathematical, Physical and Engineering Sciences, 477, 20200 824, https://doi.org/10.1098/rspa.2020.0824, 2021.

Carpenter, L. J., MacDonald, S. M., Shaw, M. D., Kumar, R., Saunders, R. W., Parthipan, R., Wilson, J., and Plane, J. M. C.: Atmospheric iodine levels influenced by sea surface emissions of inorganic iodine, Nature Geoscience, 6, 108–111, https://doi.org/https://doi.org/10.1038/ngeo1687, 2013.

Cen-Lin, H. and Tzung-May, F.: Air-Sea Exchange of Volatile Organic Compounds: A New Model with Microlayer Effects, Atmospheric and Oceanic Science Letters, 6, 97–102, https://doi.org/10.1080/16742834.2013.11447063, 2013.

Chance, R., Malin, G., Jickells, T., and Baker, A. R.: Reduction of iodate to iodide by cold water diatom cultures, Marine Chemistry, 105, 169–180, https://doi.org/https://doi.org/10.1016/j.marchem.2006.06.008, 2007.

Chance, R., Baker, A. R., Carpenter, L., and Jickells, T. D.: The distribution of iodide at the sea surface, Environ. Sci.: Processes Impacts, 16, 1841–1859, https://doi.org/10.1039/C4EM00139G, 2014.

https://doi.org/10.5194/egusphere-2023-2447
Preprint. Discussion started: 17 November 2023

Chance, R., Tinel, L., Sarkar, A., Sinha, A. K., Mahajan, A. S., Chacko, R., Sabu, P., Roy, R., Jickells, T. D., Stevens, D. P., Wadley, M., and Carpenter, L. J.: Surface Inorganic Iodine Speciation in the Indian and Southern Oceans From 12°N to 70°S, Frontiers in Marine Science, 7, https://doi.org/10.3389/fmars.2020.00621, 2020.

Chang, W., Heikes, B., and Lee, M.: Ozone deposition to the sea surface:chemical enhancement and wind speed dependence, ATMOS ENVIRON, 38, 1053–1059, https://doi.org/10.1016/j.atmosenv.2003.10.050, 2004.

Citri, O. and Epstein, I. R.: Mechanistic Study of a Coupled Chemical Oscillator: The Bromate-Chlorite Iodide Reaction, https://doi.org/10.1021/j100318a034, 1988.

Cuevas, C. A., Maffezzoli, N., Corella, J. P., Spolaor, A., Vallelonga, P., Kjær, H. A., Simonsen, M., Winstrup, M., Vinther, B., Horvat, C., Fernandez, R. P., Kinnison, D., Lamarque, J.-F., Barbante, C., and Saiz-Lopez, A.: Rapid increase in atmospheric iodine levels in the North Atlantic since the mid-20th century, Nature Communications, 9, 1452, https://doi.org/10.1038/s41467-018-03756-1, 2018.

Cuevas, C. A., Fernandez, R. P., Kinnison, D. E., Li, Q., Lamarque, J.-F., Trabelsi, T., Francisco, J. S., Solomon, S., and Saiz-Lopez, A.: The influence of iodine on the Antarctic stratospheric ozone hole, Proceedings of the National Academy of Sciences, 119, e2110864 119, https://doi.org/10.1073/pnas.2110864119, 2022.

De Barros Faria, R., Lengyel, I., Epstein, I. R., and Kustin, K.: Systematic design of chemical oscillators. 86. Combined mechanism explaining nonlinear dynamics in bromine(III) and bromine(V) oxidations of iodide ion, The Journal of Physical Chemistry, 97, 1164–1171, https://doi.org/10.1021/j100108a011, 1993.

development team, T. P.: pandas-dev/pandas: Pandas, https://doi.org/10.5281/zenodo.3509134, 2020.

Fairall, C. W., Helmig, D., Ganzeveld, L., and Hare, J.: Water-side turbulence enhancement of ozone deposition to the ocean, ATMOS CHEM PHYS, 7, 443–451, https://doi.org/10.5194/acp-7-443-2007, 2007.

Frew, N. M., Goldman, J. C., Dennett, M. R., and Johnson, A. S.: Impact of phytoplankton-generated surfactants on air-sea gas exchange, Journal of Geophysical Research: Oceans, 95, 3337–3352, https://doi.org/https://doi.org/10.1029/JC095iC03p03337, 1990.

Frieß, U., Deutschmann, T., Gilfedder, B. S., Weller, R., and Platt, U.: Iodine monoxide in the Antarctic snowpack, Atmospheric Chemistry and Physics, 10, 2439–2456, https://doi.org/10.5194/acp-10-2439-2010, 2010.

Ganzeveld, L., Helmig, D., Fairall, C., Hare, J., and Pozzer, A.: Atmosphere-ocean ozone exchange: A global modeling study of biogeochemical, atmospheric, and waterside turbulence dependencies, GLOBAL BIOGEOCHEM CY, 23, https://doi.org/10.1029/2008GB003301, 2009.

Garland, J. A., Elzerman, A. W., and Penkett, S. A.: The mechanism for dry deposition of ozone to seawater surfaces, J GEOPHYS RES-OCEANS, 85, 7488–7492, https://doi.org/10.1029/JC085iC12p07488, 1980.

GCC14.1.1: The International GEOS-Chem User Community, geoschem/GCClassic: GEOS-Chem 14.1.1, https://doi.org/10.5281/zenodo.7696651, Please see the LICENSE.txt and AUTHORS.txt files in the root folder for the GEOS-Chem license description (based on the MIT license) and a complete list of authors. For more information about GEOS-Chem in general, please see www.geos- chem.org and wiki.geos-chem.org., 2023.

Gelaro, R., McCarty, W., Suárez, M. J., Todling, R., Molod, A., Takacs, L., Randles, C. A., Darmenov, A., Bosilovich, M. G., Reichle, R., Wargan, K., Coy, L., Cullather, R., Draper, C., Akella, S., Buchard, V., Conaty, A., da Silva, A. M., Gu, W., Kim, G.-K., Koster, R., Lucchesi, R., Merkova, D., Nielsen, J. E., Partyka, G., Pawson, S., Putman, W., Rienecker, M., Schubert, S. D., Sienkiewicz, M., and Zhao, B.: The Modern-Era Retrospective Analysis for Research and Applications, Version 2 (MERRA-2), Journal of Climate, 30, 5419–5454, https://doi.org/10.1175/JCLI-D-16-0758.1, 2017.

https://doi.org/10.5194/egusphere-2023-2447
Preprint. Discussion started: 17 November 2023

Goodwin, D. G., Moffat, H. K., Schoegl, I., Speth, R. L., and Weber, B. W.: Cantera: An Object-oriented Software Toolkit for Chemical Kinetics, Thermodynamics, and Transport Processes, https://www.cantera.org, https://doi.org/10.5281/zenodo.6387882, version 2.6.0, 2022.

Großmann, K., Frieß, U., Peters, E., Wittrock, F., Lampel, J., Yilmaz, S., Tschritter, J., Sommariva, R., von Glasow, R., Quack, B., Krüger, K., Pfeilsticker, K., and Platt, U.: Iodine monoxide in the Western Pacific marine boundary layer, Atmospheric Chemistry and Physics, 13, 3363–3378, https://doi.org/10.5194/acp-13-3363-2013, 2013.

Gómez Martín, J. C., Mahajan, A. S., Hay, T. D., Prados-Román, C., Ordóñez, C., MacDonald, S. M., Plane, J. M., Sorribas, M., Gil, M., Paredes Mora, J. F., Agama Reyes, M. V., Oram, D. E., Leedham, E., and Saiz-Lopez, A.: Iodine chemistry in the eastern Pacific marine boundary layer, Journal of Geophysical Research: Atmospheres, 118, 887–904, https://doi.org/https://doi.org/10.1002/jgrd.50132, 2013.

Haag, W. R. and Hoigné, J.: Ozonation of bromide-containing waters: Kinetics of formation of hypobromous acid and bromate, Environ. Sci. Technol., 17, 261– 267, 1983.

Hao, H., Leven, I., and Head-Gordon, T.: Can electric fields drive chemistry for an aqueous microdroplet?, Nat Commun, 13, https://doi.org/10.1038/s41467-021-27941-x, 2022.

Hardacre, C., Wild, O., and Emberson, L.: An evaluation of ozone dry deposition in global scale chemistry climate models, ATMOS CHEM PHYS, 15, 6419–6436, https://doi.org/10.5194/acp-15-6419-2015, 2015.

Harris, C. R., Millman, K. J., van der Walt, S. J., Gommers, R., Virtanen, P., Cournapeau, D., Wieser, E., Taylor, J., Berg, S., Smith, N. J., Kern, R., Picus, M., Hoyer, S., van Kerkwijk, M. H., Brett, M., Haldane, A., del Río, J. F., Wiebe, M., Peterson, P., Gérard-Marchant, P., Sheppard, K., Reddy, T., Weckesser, W., Abbasi, H., Gohlke, C., and Oliphant, T. E.: Array programming with NumPy, Nature, 585, 357–362, https://doi.org/10.1038/s41586-020-2649-2, 2020.

Hoffmann, T., O'Dowd, C. D., and Seinfeld, J. H.: Iodine oxide homogeneous nucleation: An explanation for coastal new particle production, Geophysical Research Letters, 28, 1949–1952, https://doi.org/https://doi.org/10.1029/2000GL012399, 2001.

Hu, J. H., Shi, Q., Davidovits, P., Worsnop, D. R., Zahniser, M. S., and Kolb, C. E.: Reactive Uptake of Cl2(g) and Br2(g) by Aqueous Surfaces as a Function of Br- and I- Ion Concentration: The Effect of Chemical Reaction at the Interface, J. Phys. Chem., 99, 8768–8776, https://doi.org/10.1021/j100021a050, 1995.

Huang, R.-J., Hoffmann, T., Ovadnevaite, J., Laaksonen, A., Kokkola, H., Xu, W., Xu, W., Ceburnis, D., Zhang, R., Seinfeld, J. H., and O'Dowd, C.: Heterogeneous iodine-organic chemistry fast-tracks marine new particle formation, Proceedings of the National Academy of Sciences, 119, e2201729 119, https://doi.org/10.1073/pnas.2201729119, 2022.

Iglesias-Suarez, F., Badia, A., Fernandez, R. P., Cuevas, C. A., Kinnison, D. E., Tilmes, S., Lamarque, J.-F., Long, M. C., Hossaini, R., and Saiz-Lopez, A.: Natural halogens buffer tropospheric ozone in a changing climate, Nature Climate Change, 10, 147–154, https://doi.org/10.1038/s41558-019-0675-6, 2020.

Johnson, M. T.: A numerical scheme to calculate temperature and salinity dependent air-water transfer velocities for any gas, Ocean Science, 6, 913–932, https://doi.org/10.5194/os-6-913-2010, 2010.

Johnson, P. N. and Davis, R. A.: Diffusivity of Ozone in Water, J CHEM ENG DATA, 41, 1485–1487, https://doi.org/10.1021/je9602125, 1996.

Jones, C. E., Hornsby, K. E., Sommariva, R., Dunk, R. M., von Glasow, R., McFiggans, G., and Carpenter, L. J.: Quantifying the contribution of marine organic gases to atmospheric iodine, Geophysical Research Letters, 37, https://doi.org/https://doi.org/10.1029/2010GL043990, 2010.

https://doi.org/10.5194/egusphere-2023-2447
Preprint. Discussion started: 17 November 2023

Koenig, T. K., Baidar, S., Campuzano-Jost, P., Cuevas, C. A., Dix, B., Fernandez, R. P., Guo, H., Hall, S. R., Kinnison, D., Nault, B. A., Ullmann, K., Jimenez, J. L., Saiz-Lopez, A., and Volkamer, R.: Quantitative detection of iodine in the stratosphere, Proceedings of the National Academy of Sciences, 117, 1860–1866, https://doi.org/10.1073/pnas.1916828117, 2020.

Kumar, K. and Margerum, D. W.: Kinetics and mechanism of general-acid-assisted oxidation of bromide by hypochlorite and hypochlorous acid, Inorg. Chem., 26, 2706– 2711, 1987.

Kumar, K., Day, R. A., and Margerum, D. W.: Atom-transfer redox kinetics: general-acid-assisted oxidation of iodide by chloramines and hypochlorite, Inorg. Chem., 25, 4344–4350, https://doi.org/10.1021/ic00244a012, 1986.

Legrand, M., McConnell, J. R., Preunkert, S., Arienzo, M., Chellman, N., Gleason, K., Sherwen, T., Evans, M. J., and Carpenter, L. J.: Alpine ice evidence of a three-fold increase in atmospheric iodine deposition since 1950 in Europe due to increasing oceanic emissions, Proceedings of the National Academy of Sciences, 115, 12 136–12 141, https://doi.org/10.1073/pnas.1809867115, 2018.

Lengyel, I., Epstein, I. R., and Kustin, K.: Kinetics of iodine hydrolysis, Inorg. Chem., 32, 5880–5882, https://doi.org/10.1021/ic00077a036, 1993.

Lengyel, I., Li, J., Kustin, K., and Epstein, I. R.: Rate Constants for Reactions between Iodine- and Chlorine-Containing Species: A Detailed Mechanism of the Chlorine Dioxide/Chlorite-Iodide Reaction, J. Am. Chem. Soc., pp. 3708–3719, https://doi.org/https://doi.org/10.1021/ja953938e, 1996.

Levanov, A. V., Isaikina, O. Y., Gasanova, R. B., Uzhel, A. S., and Lunin, V. V.: Kinetics of chlorate formation during ozonation of aqueous chloride solutions, Chemosphere, 229, 68–76, https://doi.org/https://doi.org/10.1016/j.chemosphere.2019.04.105, 2019.

Liu, Q., Schurter, L. M., Muller, C. E., Aloisio, S., Francisco, J. S., and Margerum, D. W.: Kinetics and Mechanisms of Aqueous Ozone Reactions with Bromide, Sulfite, Hydrogen Sulfite, Iodide, and Nitrite Ions, INORG CHEM, 40, 4436–4442, https://doi.org/10.1021/ic000919j, 2001.

Luhar, A. K., Galbally, I. E., Woodhouse, M. T., and Thatcher, M.: An improved parameterisation of ozone dry deposition to the ocean and its impact in a global climate-chemistry model, ATMOS CHEM PHYS, 17, 3749–3767, https://doi.org/10.5194/acp-17-3749-2017, 2017.

Luhar, A. K., Woodhouse, M. T., and Galbally, I. E.: A revised global ozone dry deposition estimate based on a new two-layer parameterisation for air–sea exchange and the multi-year MACC composition reanalysis, ATMOS CHEM PHYS, 18, 4329–4348, https://doi.org/10.5194/acp-18-4329-2018, 2018.

MacDonald, S. M., Gómez Martín, J. C., Chance, R., Warriner, S., Saiz-Lopez, A., Carpenter, L. J., and Plane, J. M. C.: A laboratory characterisation of inorganic iodine emissions from the sea surface: dependence on oceanic variables and parameterisation for global modelling, ATMOS CHEM PHYS, 14, 5841–5852, https://doi.org/10.5194/acp-14-5841-2014, 2014.

Magi, L., Schweitzer, F., Pallares, C., Cherif, S., Mirabel, P., and George, C.: Investigation of the Uptake Rate of Ozone and Methyl Hydroperoxide by Water Surfaces, J PHYS CHEM A, 101, 4943–4949, https://doi.org/10.1021/jp970646m, 1997.

Mahajan, A. S., Plane, J. M. C., Oetjen, H., Mendes, L., Saunders, R. W., Saiz-Lopez, A., Jones, C. E., Carpenter, L. J., and McFiggans, G. B.: Measurement and modelling of tropospheric reactive halogen species over the tropical Atlantic Ocean, Atmospheric Chemistry and Physics, 10, 4611–4624, https://doi.org/10.5194/acp-10-4611-2010, 2010.

Mahajan, A. S., Gómez Martín, J. C., Hay, T. D., Royer, S.-J., Yvon-Lewis, S., Liu, Y., Hu, L., Prados-Roman, C., Ordóñez, C., Plane, J. M. C., and Saiz-Lopez, A.: Latitudinal distribution of reactive iodine in the Eastern Pacific and its link to open ocean sources, Atmospheric Chemistry and Physics, 12, 11 609–11 617, https://doi.org/10.5194/acp-12-11609-2012, 2012.

https://doi.org/10.5194/egusphere-2023-2447
Preprint. Discussion started: 17 November 2023

Mahajan, A. S., Biswas, M. S., Beirle, S., Wagner, T., Schönhardt, A., Benavent, N., and Saiz-Lopez, A.: Observations of iodine monoxide over three summers at the Indian Antarctic bases of Bharati and Maitri, Atmospheric Chemistry and Physics, 21, 11 829–11 842, https://doi.org/10.5194/acp-21-11829-2021, 2021.

Michalowski, B. A., Francisco, J. S., Li, S.-M., Barrie, L. A., Bottenheim, J. W., and Shepson, P. B.: A computer model study of multiphase chemistry in the Arctic boundary layer during polar sunrise, Journal of Geophysical Research: Atmospheres, 105, 15 131–15 145, https://doi.org/https://doi.org/10.1029/2000JD900004, 2000.

Moreno, C. G., Gálvez, O., López-Arza Moreno, V., Espildora-García, E. M., and Baeza-Romero, M. T.: A revisit of the interaction of gaseous ozone with aqueous iodide. Estimating the contributions of the surface and bulk reactions, Phys. Chem. Chem. Phys., 20, 27 571–27 584, https://doi.org/10.1039/C8CP04394A, 2018.

Morris, J.: The aqueous solubility of ozone - A review, Ozone news, 1, 14–16, 1988.

Nagy, J. C., Kumar, K., and Margerum, D. W.: Non-Metal Redox Kinetics: Oxidation of Iodide by Hypochlorous Acid and by Nitrogen Trichloride Measured by the Pulsed-Accelerated-Flow Method, Inorg. Chem., 27, 2773–2780, https://doi.org/10.1021/ic00289a007, 1988.

Nightingale, P. D., Malin, G., Law, C. S., Watson, A. J., Liss, P. S., Liddicoat, M. I., Boutin, J., and Upstill-Goddard, R. C.: In situ evaluation of air-sea gas exchange parameterizations using novel conservative and volatile tracers, Global Biogeochemical Cycles, 14, 373–387, https://doi.org/https://doi.org/10.1029/1999GB900091, 2000.

Ordóñez, C., Lamarque, J.-F., Tilmes, S., Kinnison, D. E., Atlas, E. L., Blake, D. R., Sousa Santos, G., Brasseur, G., and Saiz-Lopez, A.: Bromine and iodine chemistry in a global chemistry-climate model: description and evaluation of very short-lived oceanic sources, Atmospheric Chemistry and Physics, 12, 1423–1447, https://doi.org/10.5194/acp-12-1423-2012, 2012.

Paquette, J.: Modelling the chemistry of iodine, Proceedings of the CSNI workshop on iodine chemistry in reactor safety (2nd : 1988 : Toronto), pp. 216–234, https://doi.org/https://www.oecd-nea.org/jcms/pl_15816/proceedings-of-the-csni-workshop-on-iodine-chemistry-in-reactor-safety-2nd-1988-toronto-1989?details=true, 1989.

Pound, R., Brown, L., Evans, M., and Carpenter, L.: Coupled Ocean-Atmosphere Gas Exchange Model, https://doi.org/10.5281/zenodo.10018582, Please see the LICENSE.txt in the root folder for the license description (MIT license), 2023a.

Pound, R., Brown, L., Evans, M., and Carpenter, L.: Coupled Ocean Atmosphere Gas Exchange Model Sensitivity Analysis, https://doi.org/10.15124/e377ffa4-ede9-490d-8a65-95f3b6d61137, 2023b.

Pound, R. J., Sherwen, T., Helmig, D., Carpenter, L. J., and Evans, M. J.: Influences of oceanic ozone deposition on tropospheric photochemistry, Atmospheric Chemistry and Physics, 20, 4227–4239, https://doi.org/10.5194/acp-20-4227-2020, 2020.

Pound, R. J., Durcan, D. P., Evans, M. J., and Carpenter, L. J.: Comparing the Importance of Iodine and Isoprene on Tropospheric Photochemistry, Geophysical Research Letters, 50, e2022GL100 997, https://doi.org/https://doi.org/10.1029/2022GL100997, 2023c.

Prados-Roman, C., Cuevas, C. A., Hay, T., Fernandez, R. P., Mahajan, A. S., Royer, S.-J., Galí, M., Simó, R., Dachs, J., Großmann, K., Kinnison, D. E., Lamarque, J.-F., and Saiz-Lopez, A.: Iodine oxide in the global marine boundary layer, Atmospheric Chemistry and Physics, 15, 583–593, https://doi.org/10.5194/acp-15-583-2015, 2015.

Reeser, D. and Donaldson, D.: Influence of water surface properties on the heterogeneous reaction between O3(g) and I(aq)-, Atmospheric Environment, 45, 6116–6120, https://doi.org/10.1016/j.atmosenv.2011.08.042, 2011.

Rouvière, A. and Ammann, M.: The effect of fatty acid surfactants on the uptake of ozone to aqueous halogenide particles, Atmospheric Chemistry and Physics, 10, 11 489–11 500, https://doi.org/10.5194/acp-10-11489-2010, 2010.

https://doi.org/10.5194/egusphere-2023-2447
Preprint. Discussion started: 17 November 2023

Saiz-Lopez, A., Mahajan, A. S., Salmon, R. A., Bauguitte, S. J.-B., Jones, A. E., Roscoe, H. K., and Plane, J. M. C.: Boundary Layer Halogens in Coastal Antarctica, Science, 317, 348–351, https://doi.org/10.1126/science.1141408, 2007.

Saiz-Lopez, A., Baidar, S., Cuevas, C. A., Koenig, T. K., Fernandez, R. P., Dix, B., Kinnison, D. E., Lamarque, J.-F., Rodriguez-Lloveras, X., Campos, T. L., and Volkamer, R.: Injection of iodine to the stratosphere, Geophysical Research Letters, 42, 6852–6859, https://doi.org/https://doi.org/10.1002/2015GL064796, 2015.

Schmidt, J. A., Jacob, D. J., Horowitz, H. M., Hu, L., Sherwen, T., Evans, M. J., Liang, Q., Suleiman, R. M., Oram, D. E., Le Breton, M., Percival, C. J., Wang, S., Dix, B., and Volkamer, R.: Modeling the observed tropospheric BrO background: Importance of multiphase chemistry and implications for ozone, OH, and mercury, J GEOPHYS RES-ATMOS, 121, 11,819–11,835, https://doi.org/10.1002/2015JD024229, 2016.

Schneider, S. R., Lakey, P. S. J., Shiraiwa, M., and Abbatt, J. P. D.: Reactive Uptake of Ozone to Simulated Seawater: Evidence for Iodide Depletion, The Journal of Physical Chemistry A, 124, 9844–9853, https://doi.org/10.1021/acs.jpca.0c08917, 2020.

Schneider, S. R., Lakey, P. S. J., Shiraiwa, M., and Abbatt, J. P. D.: Iodine emission from the reactive uptake of ozone to simulated seawater, Environ. Sci.: Processes Impacts, 25, 254–263, https://doi.org/10.1039/D2EM00111J, 2023.

Sebők-Nagy, K. and Körtvélyesi, T.: Kinetics and mechanism of the hydrolytic disproportionation of iodine, International Journal of Chemical Kinetics, 36, 596–602, https://doi.org/https://doi.org/10.1002/kin.20033, 2004.

Shaw, M. D. and Carpenter, L. J.: Modification of Ozone Deposition and I2 Emissions at the Air–Aqueous Interface by Dissolved Organic Carbon of Marine Origin, Environ. Sci. Technol., 47, 10 947–10 954, https://doi.org/10.1021/es4011459, 2013.

Sherwen, T., Evans, M. J., Carpenter, L. J., Andrews, S. J., Lidster, R. T., Dix, B., Koenig, T. K., Sinreich, R., Ortega, I., Volkamer, R., Saiz-Lopez, A., Prados-Roman, C., Mahajan, A. S., and Ordóñez, C.: Iodine's impact on tropospheric oxidants: a global model study in GEOS-Chem, Atmospheric Chemistry and Physics, 16, 1161–1186, https://doi.org/10.5194/acp-16-1161-2016, 2016.

Sherwen, T., Chance, R. J., Tinel, L., Ellis, D., Evans, M. J., and Carpenter, L. J.: A machine-learning-based global sea-surface iodide distribution, EARTH SYST SCI DATA, 11, 1239–1262, https://doi.org/10.5194/essd-11-1239-2019, 2019.

Smith, S. D.: Wind stress and heat flux over the ocean in gale force winds, J. Phys. Oceanogr., 10, 709–726, 1980.

Sommariva, R., Bloss, W., and von Glasow, R.: Uncertainties in gas-phase atmospheric iodine chemistry, Atmospheric Environment, 57, 219–232, https://doi.org/https://doi.org/10.1016/j.atmosenv.2012.04.032, 2012.

Tham, Y. J., He, X.-C., Li, Q., Cuevas, C. A., Shen, J., Kalliokoski, J., Yan, C., Iyer, S., Lehmusjärvi, T., Jang, S., Thakur, R. C., Beck, L., Kemppainen, D., Olin, M., Sarnela, N., Mikkilä, J., Hakala, J., Marbouti, M., Yao, L., Li, H., Huang, W., Wang, Y., Wimmer, D., Zha, Q., Virkanen, J., Spain, T. G., O'Doherty, S., Jokinen, T., Bianchi, F., Petäjä, T., Worsnop, D. R., Mauldin, R. L., Ovadnevaite, J., Ceburnis, D., Maier, N. M., Kulmala, M., O'Dowd, C., Maso, M. D., Saiz-Lopez, A., and Sipilä, M.: Direct field evidence of autocatalytic iodine release from atmospheric aerosol, Proceedings of the National Academy of Sciences, 118, e2009951 118, https://doi.org/10.1073/pnas.2009951118, 2021.

Tinel, L., Adams, T. J., Hollis, L. D. J., Bridger, A. J. M., Chance, R. J., Ward, M. W., Ball, S. M., and Carpenter, L. J.: Influence of the Sea Surface Microlayer on Oceanic Iodine Emissions, Environmental Science and Technology, https://doi.org/https://doi.org/10.1021/acs.est.0c02736, 2020.

Truesdale, V. W. and Jones, K.: Steady-state mixing of iodine in shelf seas off the British Isles, Continental Shelf Research, 20, 1889–1905, https://doi.org/https://doi.org/10.1016/S0278-4343(00)00050-9, 2000.

Tsilingiris, P.: Thermophysical and transport properties of humid air at temperature range between 0 and 100°C, Energy Conversion and Management, 49, 1098–1110, https://doi.org/https://doi.org/10.1016/j.enconman.2007.09.015, 2008.

https://doi.org/10.5194/egusphere-2023-2447
Preprint. Discussion started: 17 November 2023

Virtanen, P., Gommers, R., Oliphant, T. E., Haberland, M., Reddy, T., Cournapeau, D., Burovski, E., Peterson, P., Weckesser, W., Bright, J., van der Walt, S. J., Brett, M., Wilson, J., Millman, K. J., Mayorov, N., Nelson, A. R. J., Jones, E., Kern, R., Larson, E., Carey, C. J., Polat, İ., Feng, Y., Moore, E. W., VanderPlas, J., Laxalde, D., Perktold, J., Cimrman, R., Henriksen, I., Quintero, E. A., Harris, C. R., Archibald, A. M., Ribeiro, A. H., Pedregosa, F., van Mulbregt, P., and SciPy 1.0 Contributors: SciPy 1.0: Fundamental Algorithms for Scientific Computing in Python, Nature Methods, 17, 261–272, https://doi.org/10.1038/s41592-019-0686-2, 2020.

Wadley, M. R., Stevens, D. P., Jickells, T. D., Hughes, C., Chance, R., Hepach, H., Tinel, L., and Carpenter, L. J.: A Global Model for Iodine Speciation in the Upper Ocean, Global Biogeochemical Cycles, 34, e2019GB006 467, https://doi.org/https://doi.org/10.1029/2019GB006467, 2020.

Wang, T. X. and Margerum, D. W.: Kinetics of reversible chlorine hydrolysis: Temperature-dependence and general acid/base assisted mechanisms, Inorg. Chem., 33, 1050– 1055, https://doi.org/https://doi.org/10.1021/ic00084a014, 1994.

Wang, T. X., Kelley, M. D., Cooper, J. N., Beckwith, R. C., and Margerum, D. W.: Equilibrium, kinetic and UV-spectral characteristics of aqueous bromine chloride, bromine and chlorine species, Inorg. Chem., 33, 5872– 5878, https://doi.org/https://doi.org/10.1021/ic00103a040, 1994.

Wang, X., Jacob, D. J., Downs, W., Zhai, S., Zhu, L., Shah, V., Holmes, C. D., Sherwen, T., Alexander, B., Evans, M. J., Eastham, S. D., Neuman, J. A., Veres, P. R., Koenig, T. K., Volkamer, R., Huey, L. G., Bannan, T. J., Percival, C. J., Lee, B. H., and Thornton, J. A.: Global tropospheric halogen (Cl, Br, I) chemistry and its impact on oxidants, Atmospheric Chemistry and Physics, 21, 13 973–13 996, https://doi.org/10.5194/acp-21-13973-2021, 2021.

Wang, Y. L., Nagy, J. C., and Margerum, D.: Kinetics of hydrolysis of iodine monochloride measured by the pulsed-accelerated-flow method, J. Am. Chem. Soc., pp. 7838–7844, https://doi.org/10.1021/ja00202a026, 1989.

Wesely, M. and Hicks, B.: Some Factors that Affect the Deposition Rates of Sulfur Dioxide and Similar Gases on Vegetation, Journal of the Air Pollution Control Association, 27, 1110–1116, https://doi.org/10.1080/00022470.1977.10470534, 1977.

Xiong, H., Lee, J., Zare, R., and Min, W.: Strong Electric Field Observed at the Interface of Aqueous Microdroplets, J Phys Chem Lett, https://doi.org/10.1021/acs.jpclett.0c02061, 2020.

Young, P. J., Archibald, A. T., Bowman, K. W., Lamarque, J.-F., Naik, V., Stevenson, D. S., Tilmes, S., Voulgarakis, A., Wild, O., Bergmann, D., Cameron-Smith, P., Cionni, I., Collins, W. J., Dalsøren, S. B., Doherty, R. M., Eyring, V., Faluvegi, G., Horowitz, L. W., Josse, B., Lee, Y. H., MacKenzie, I. A., Nagashima, T., Plummer, D. A., Righi, M., Rumbold, S. T., Skeie, R. B., Shindell, D. T., Strode, S. A., Sudo, K., Szopa, S., and Zeng, G.: Pre-industrial to end 21st century projections of tropospheric ozone from the Atmospheric Chemistry and Climate Model Intercomparison Project (ACCMIP), ATMOS CHEM PHYS, 13, 2063–2090, https://doi.org/10.5194/acp-13-2063-2013, 2013.

https://doi.org/10.5194/egusphere-2023-2447
Preprint. Discussion started: 17 November 2023

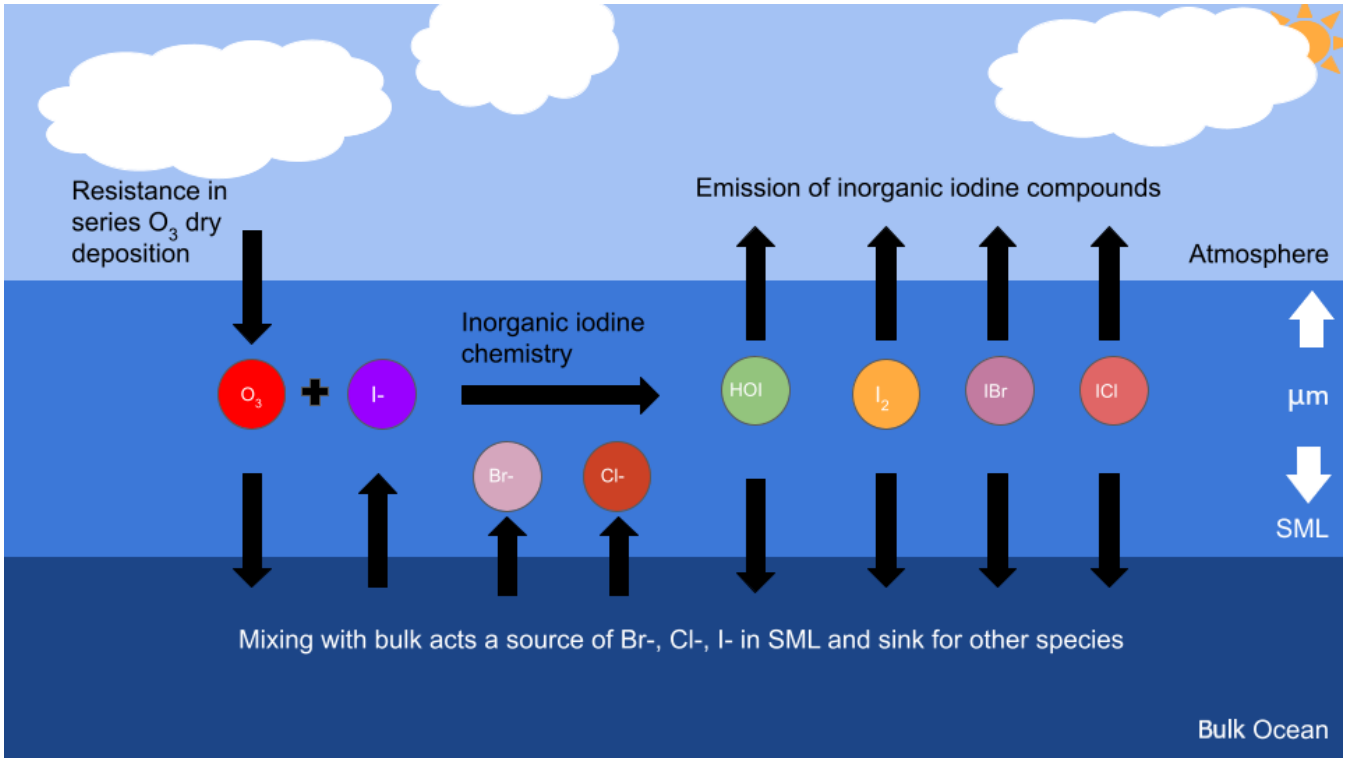

Figure 1. Overview diagram describing the physical arrangement of the ocean surface microlayer and the key chemical species included in the model The black arrows represent the chemical fluxes and their net direction in this model.

https://doi.org/10.5194/egusphere-2023-2447
Preprint. Discussion started: 17 November 2023

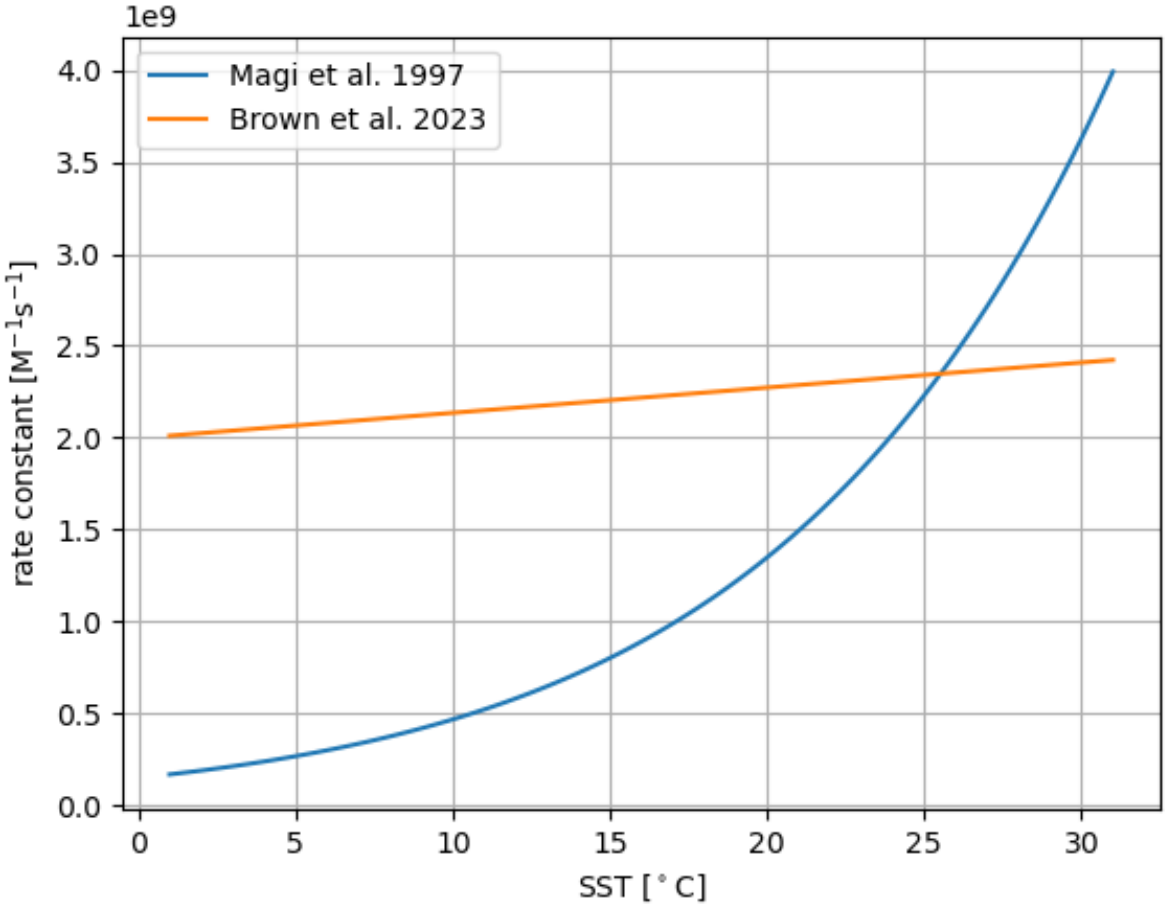

Figure 2. Comparison of the two published temperature-dependent rate coefficients from Magi et al. (1997) (blue) and Brown et al. (2023) (orange)

https://doi.org/10.5194/egusphere-2023-2447
Preprint. Discussion started: 17 November 2023

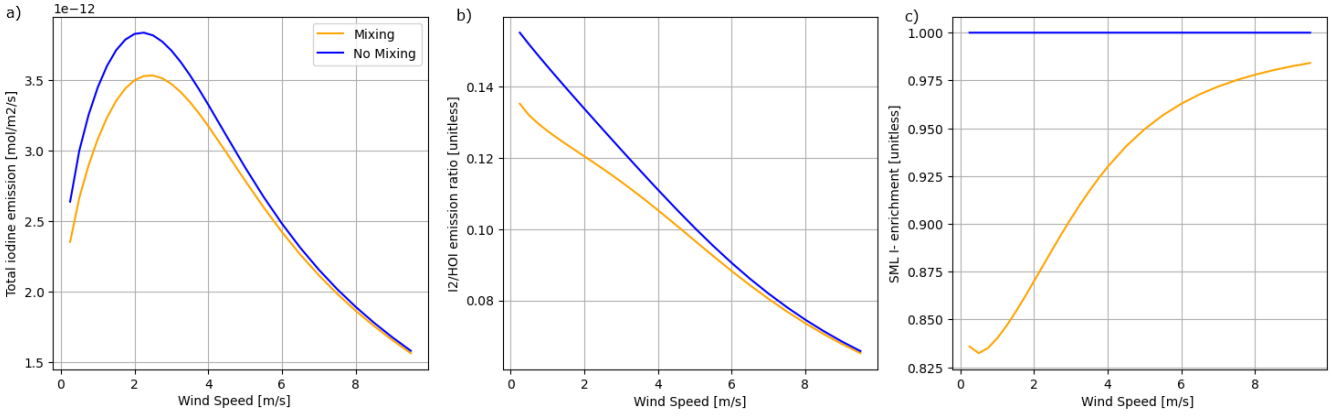

Figure 3. Comparisons of the SML model predictions with no mixing of I^- (100 nM in both the SML and bulk layers) (blue) and mixing of I^- from the bulk layer and varying in the SML (orange). a) Total inorganic iodine emission (HOI+I_2+IBr+ICl) vs wind speed, b) The ratio of I_2/HOI emission vs wind speed and c) SML I^- enrichment (SML concentration/bulk concentration) vs wind speed. All calculations are performed at 30 ppb of atmospheric O_3, 100 nM I^- concentration in bulk water, and 285K sea surface temperature (SST).

https://doi.org/10.5194/egusphere-2023-2447
Preprint. Discussion started: 17 November 2023

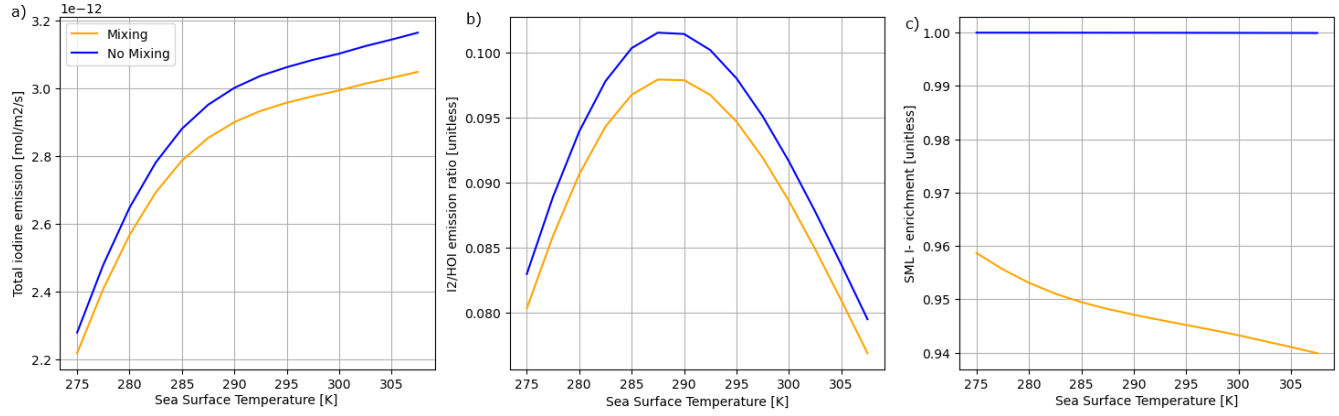

Figure 4. Comparisons of the SML model predictions with no mixing of I^- (100 nM in both the SML and bulk layers) (blue) and mixing of I^- from the bulk layer and varying concentration in the SML (orange). a) Total inorganic iodine emission (HOI+I_2+IBr+ICl) vs SST, b) The ratio of I_2/HOI emission vs SST and c) SML I^- enrichment (SML concentration/bulk concentration) vs SST. All calculated at 30 ppb of atmospheric O_3, 100 nM I^- concentration in bulk water, and 5 ms^{-1} wind speed.

https://doi.org/10.5194/egusphere-2023-2447
Preprint. Discussion started: 17 November 2023

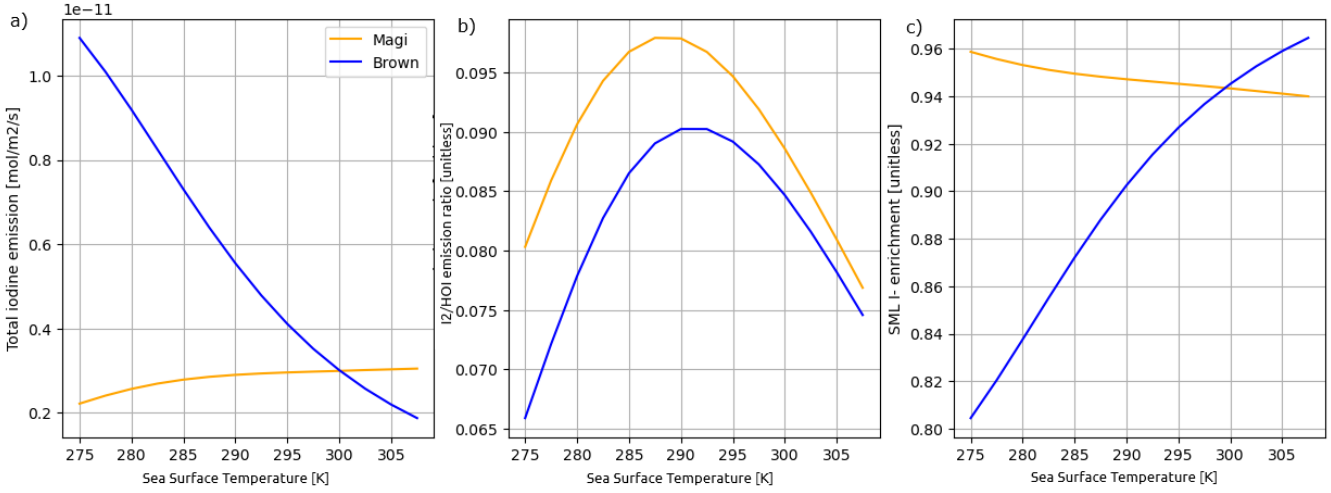

Figure 5. Comparisons of the SML model with the I^- + O_3 rate reported by Magi et al. (1997) (orange) and Brown et al. (2023) (blue). a) Total inorganic iodine emission vs SST, b) the ratio of I_2/HOI emission vs SST and c) SML I- enrichment (SML concentration / bulk concentration) vs SST. All are calculated at 30 ppb of atmospheric O_3, 5m/s wind speed, and 100 nM I^- concentration in bulk water.

https://doi.org/10.5194/egusphere-2023-2447
Preprint. Discussion started: 17 November 2023

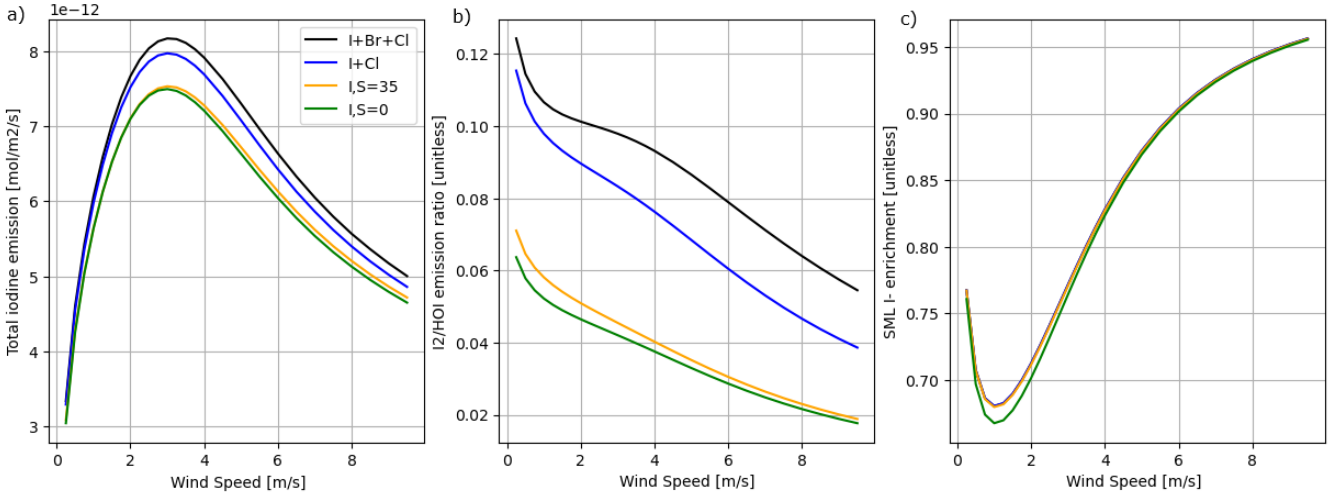

Figure 6. Comparisons of the SML model with only iodine chemistry (green), only iodine chemistry but with a salinity of 35 PSU (orange), iodine and chlorine chemistry (blue), and with the full chemistry scheme present (iodine, bromine and chlorine chemistry, black). a) shows total inorganic iodine emission vs SST, b) ratio of I_2/HOI emission vs SST and c) SML I- enrichment (SML concentration/bulk concentration) vs SST. All calculated at 30 ppb of atmospheric O_3, 5 ms^{-1} wind speed, and 100 nM I^- concentration in bulk water.

https://doi.org/10.5194/egusphere-2023-2447
Preprint. Discussion started: 17 November 2023

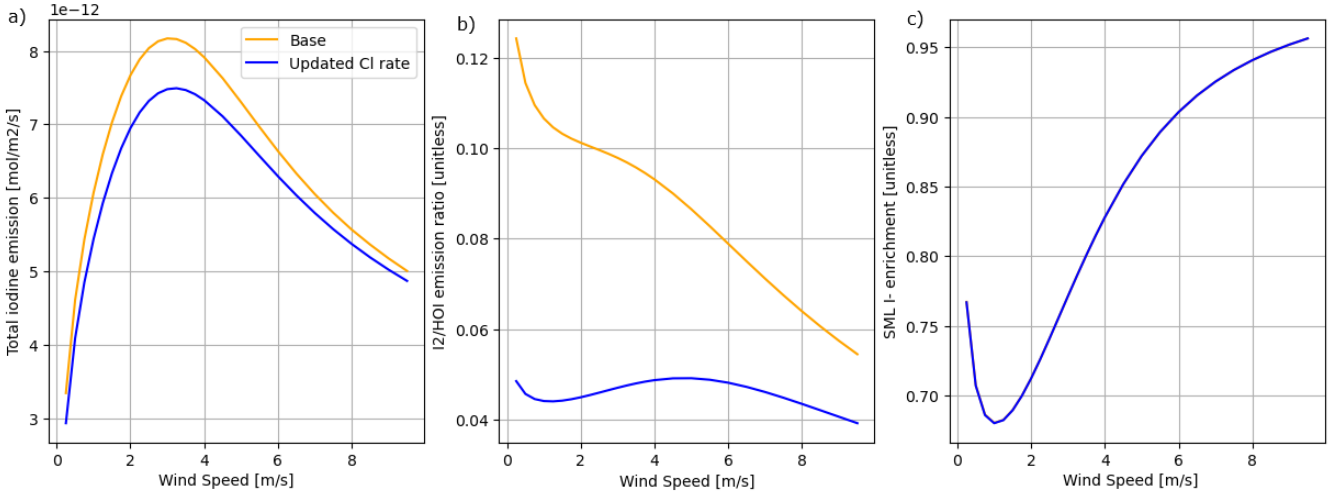

Figure 7. Comparisons of the SML model with $I^- + O_3$ rate using the standard chemistry scheme (orange) and the updated equilibrium from Schneider et al. (2023) (blue). a) shows total inorganic iodine emission vs SST, b) ratio of I_2/HOI emission vs SST and c) SML I- enrichment (SML concentration/bulk concentration) vs SST all using 30ppbv of atmospheric O_3, 5m/s wind speed, and 100 nM I^-.

https://doi.org/10.5194/egusphere-2023-2447
Preprint. Discussion started: 17 November 2023

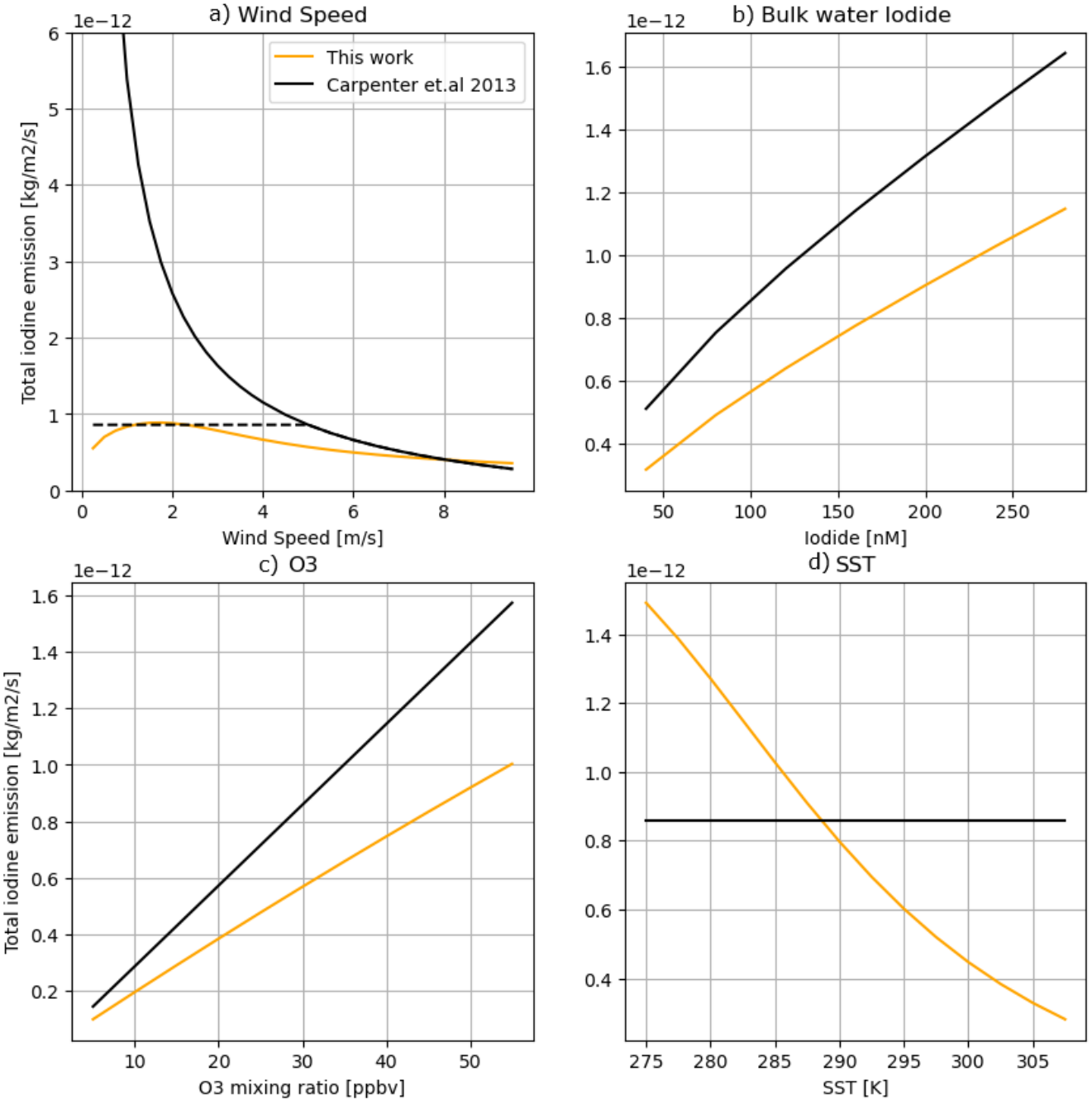

Figure 8. Comparison between total iodine emissions from this work and the model as implemented by Carpenter et al. (2013) across a range of wind speeds (a) (both with (dashed black line) and without (solid black line) a minimum wind speed of 5.5 ms^{-1}), bulk water iodide concentrations (b), atmospheric O_3 mixing ratios (c) and sea surface temperatures (d)

https://doi.org/10.5194/egusphere-2023-2447
Preprint. Discussion started: 17 November 2023

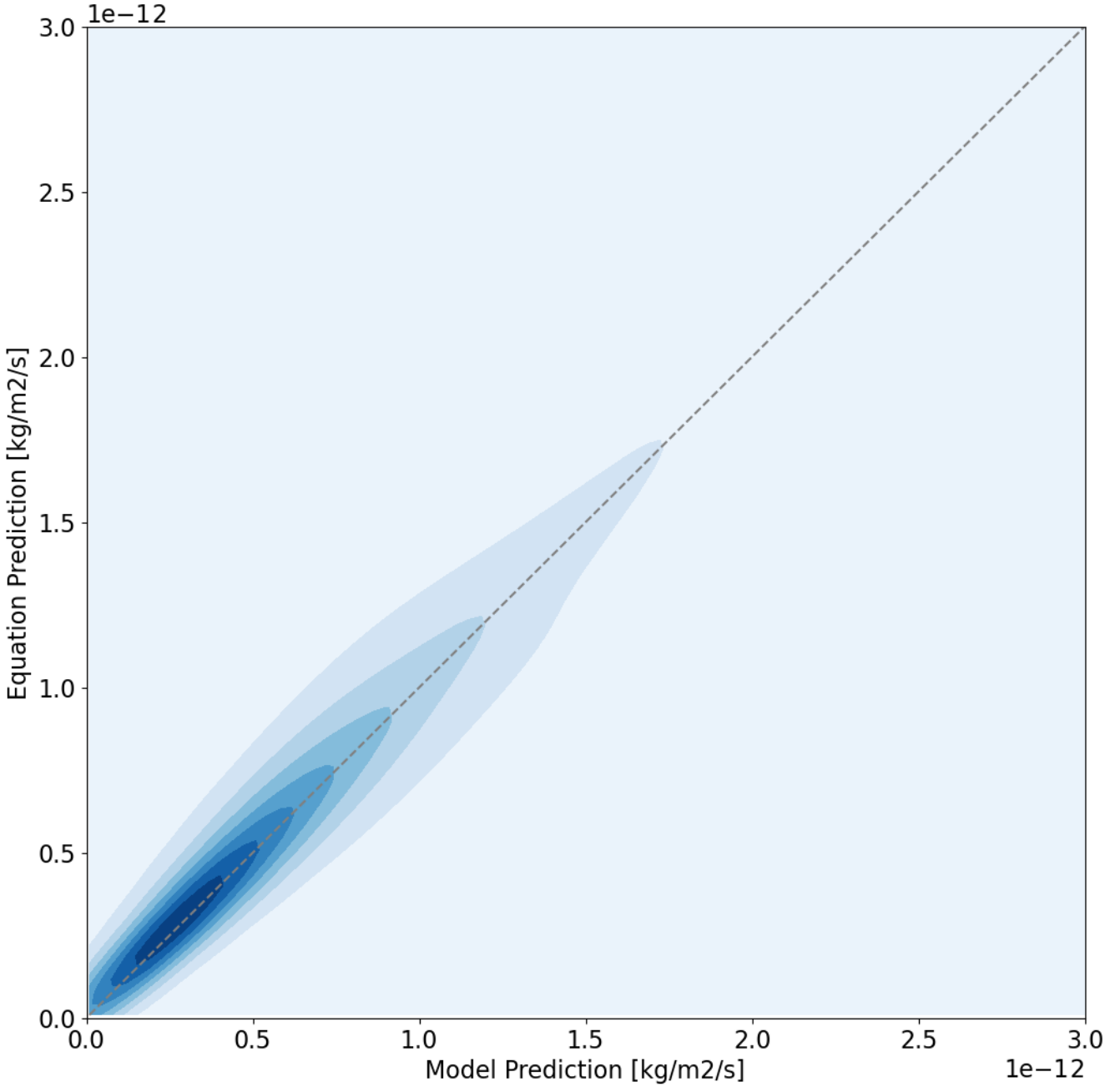

Figure 9. Correlation between modelled total inorganic iodine emission and the sum of HOI + I_2 predicted using equations 17 and 18

https://doi.org/10.5194/egusphere-2023-2447
Preprint. Discussion started: 17 November 2023

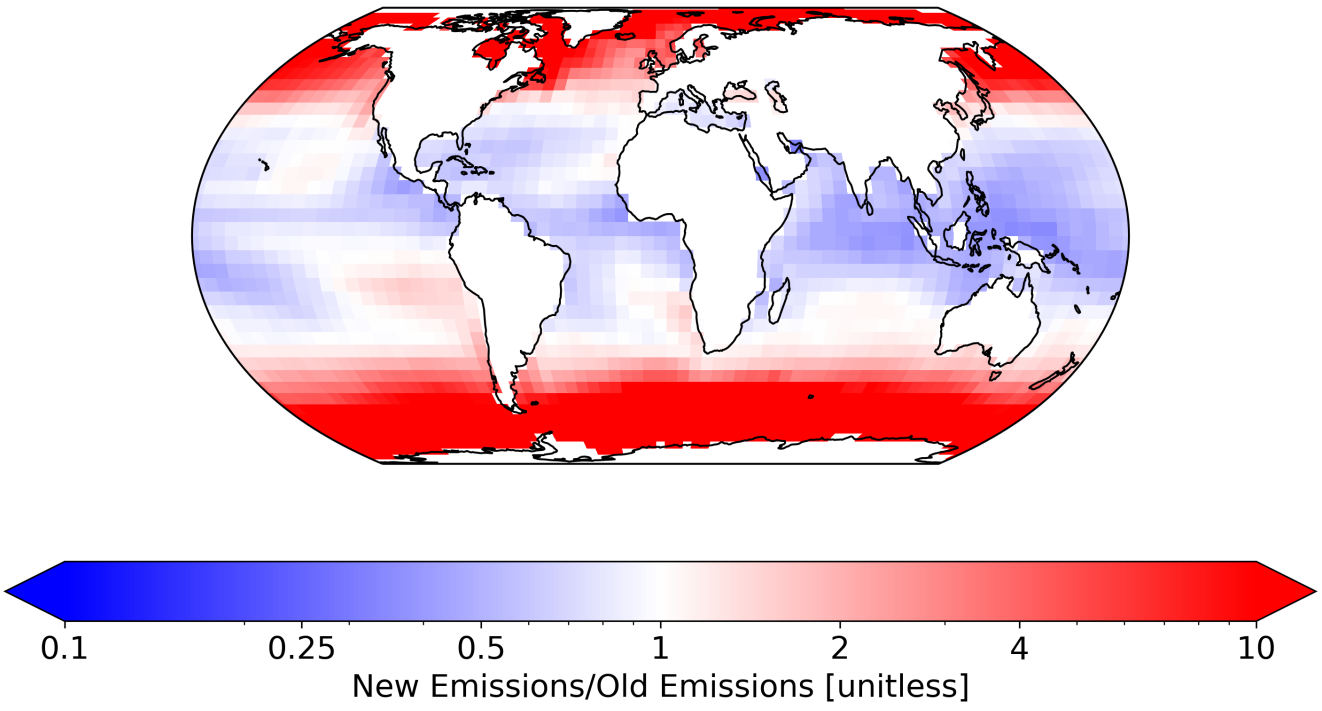

Figure 10. Fractional change in the annual mean total inorganic iodine emissions from Carpenter et al. (2013) equations and MacDonald et al. (2014) I^- to the new HOI and I_2 emission equations (equations 17 and 18) and Sherwen et al. (2019) I^-. The new version of inorganic iodine emission equations combined with Sherwen et al. (2019) sea surface iodide predicts higher emissions at higher latitudes and a decrease in emissions from warmer, tropical waters.

https://doi.org/10.5194/egusphere-2023-2447
Preprint. Discussion started: 17 November 2023

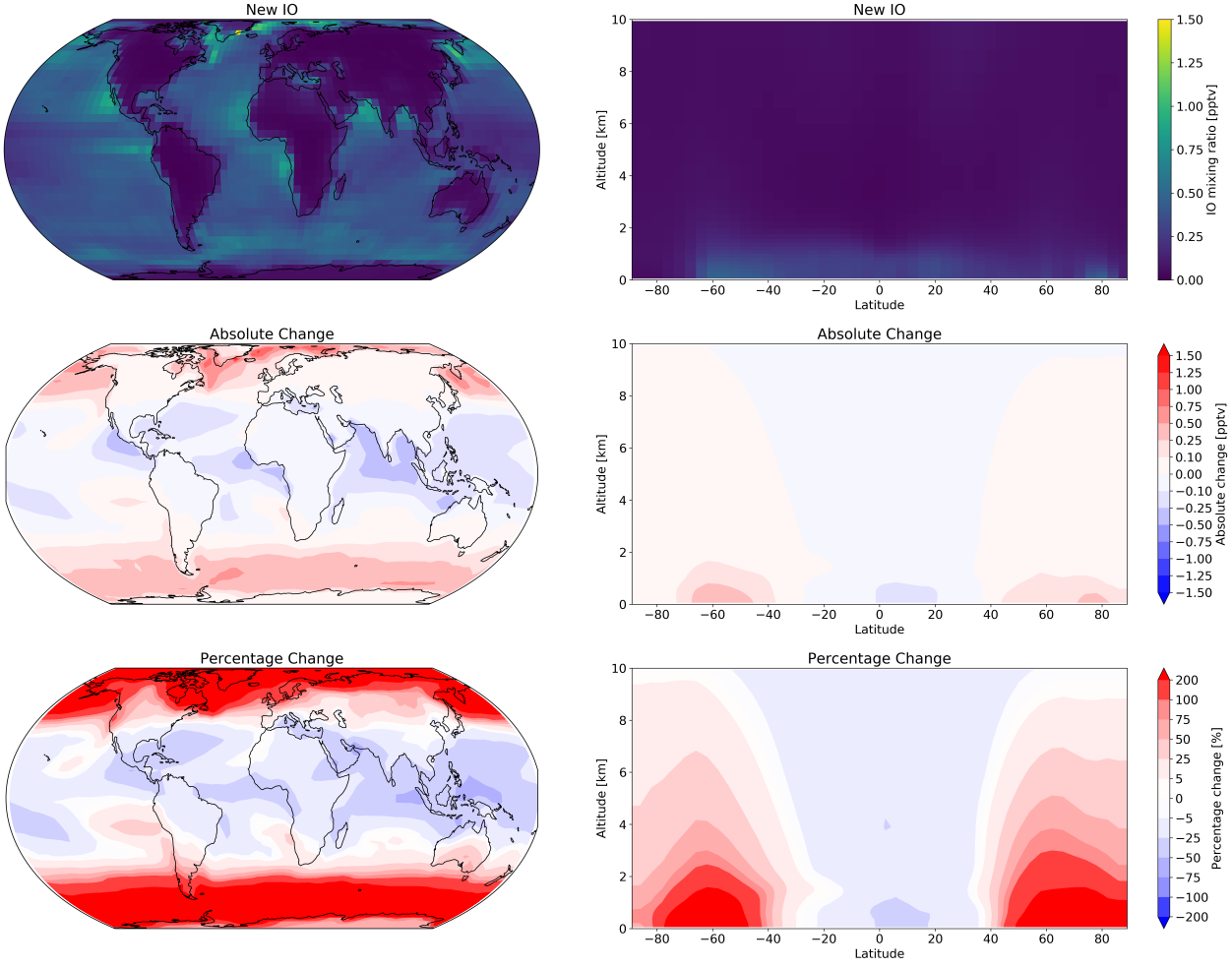

Figure 11. Annual mean mixing ratio of IO (top) using new inorganic iodine emissions, absolute change (middle) and percentage change (bottom) in the annual mean atmospheric IO from implementing the new inorganic iodine emissions.

https://doi.org/10.5194/egusphere-2023-2447
Preprint. Discussion started: 17 November 2023

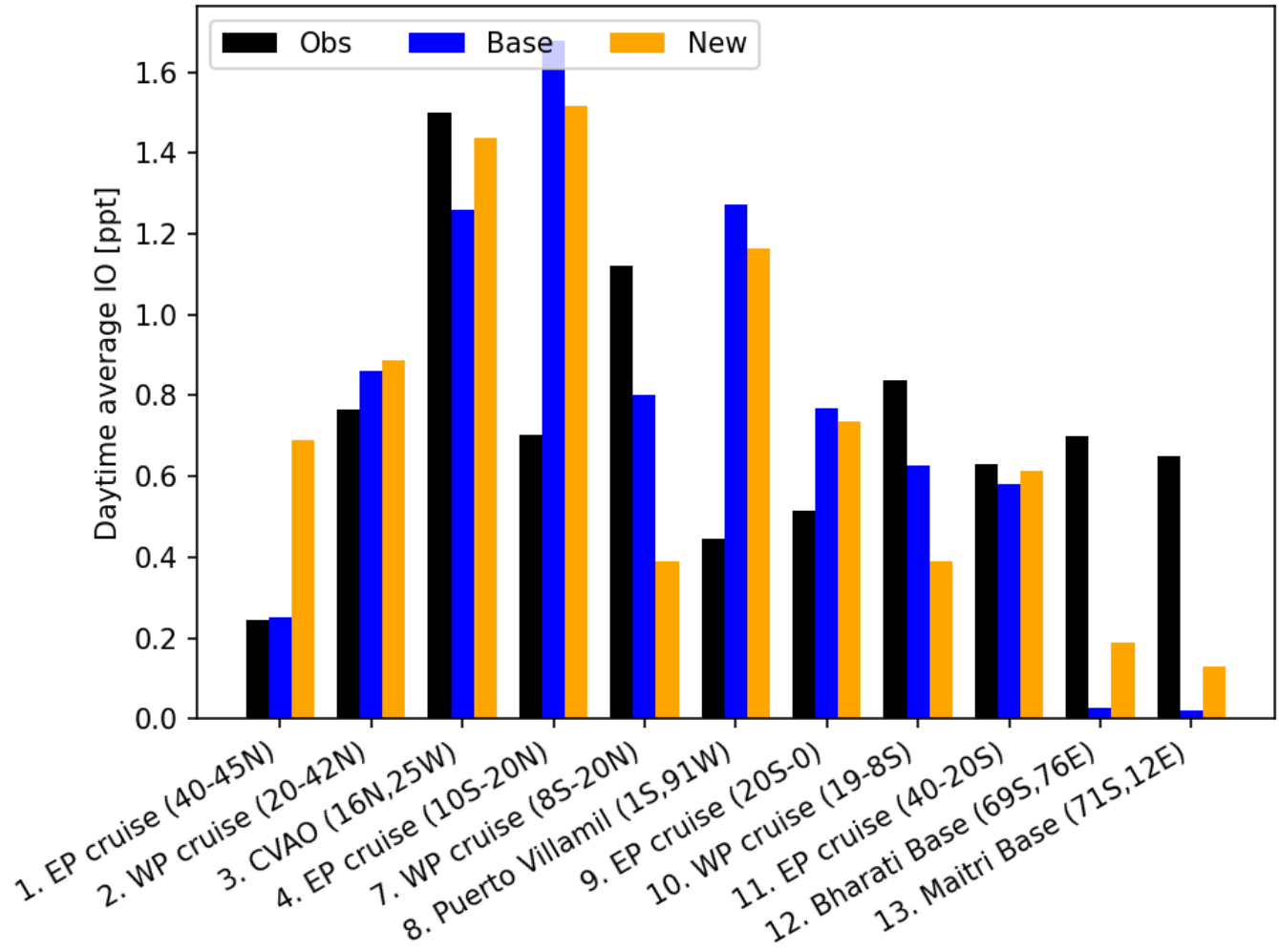

Figure 12. Daytime surface average IO mixing ratio from coastal sites and ocean cruises with observations (black) from reporting periods in different years. Model values are monthly mean daytime surface values taken from the same reporting month and location but from years 2020/21 where the base (blue) uses HOI and I_2 emissions from Carpenter et al. (2013) and new (orange) uses the HOI and I_2 emissions presented in this work. References: (1, 4, 9, 11) Mahajan et al. (2012), (2, 7, 10) Großmann et al. (2013), (3) Mahajan et al. (2010), (8) Gómez Martín et al. (2013), (12, 13) Mahajan et al. (2021)

https://doi.org/10.5194/egusphere-2023-2447
Preprint. Discussion started: 17 November 2023

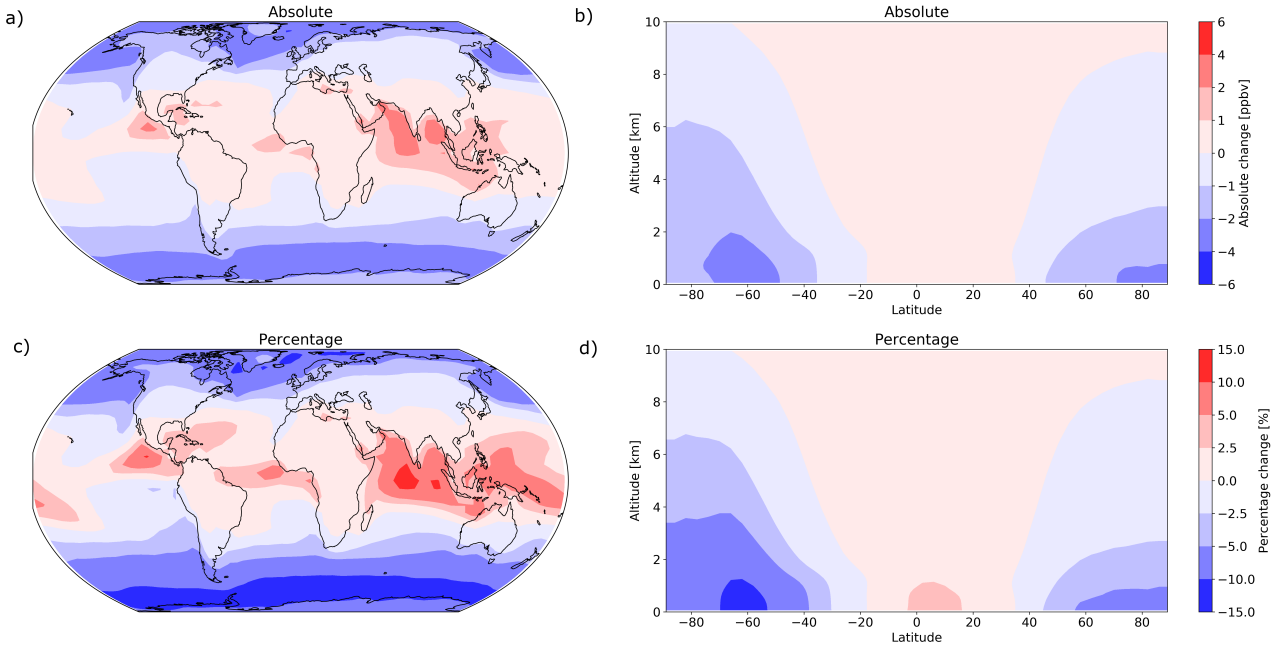

Figure 13. Absolute and percentage change in surface O_3 (a and c), absolute and percentage change in zonal O_3 (b and d). The largest changes occur in the surface levels of the model, with the largest relative decrease in surface O_3 occurring over the Southern Ocean and the largest relative increase occurring over the Indian Ocean.

https://doi.org/10.5194/egusphere-2023-2447
Preprint. Discussion started: 17 November 2023

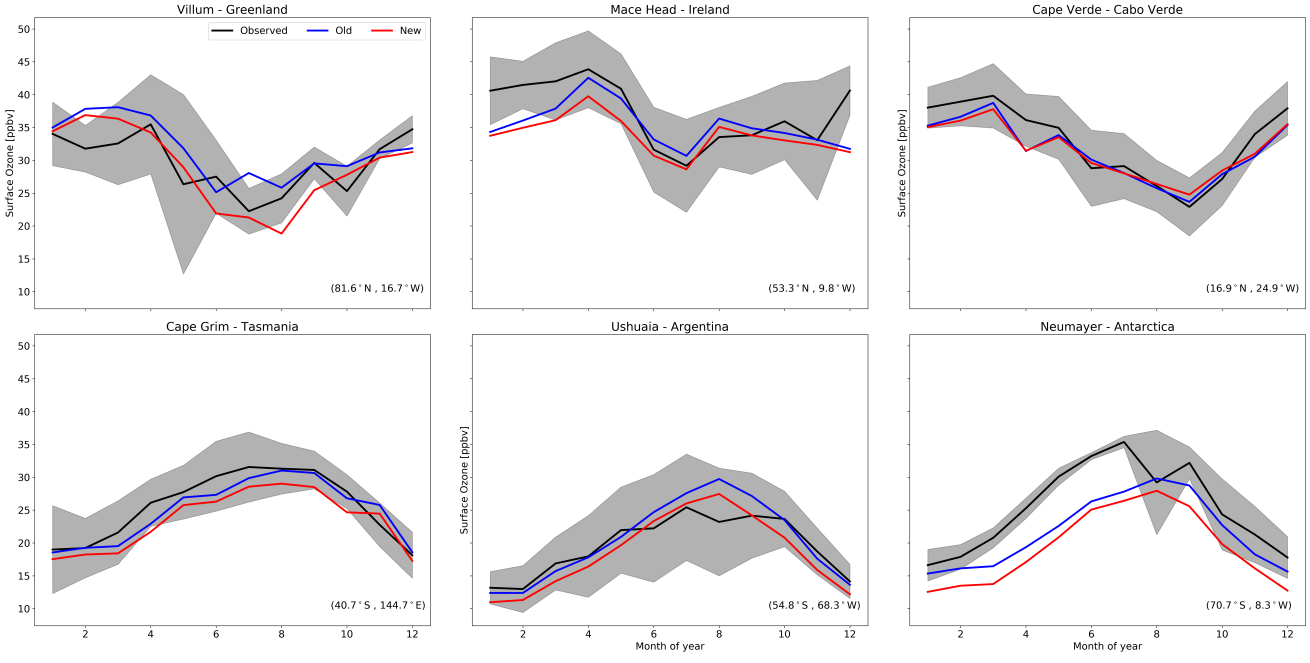

Figure 14. Predictions and observations of monthly average surface ozone mixing ratio from the model using the old iodine emissions (old) and the model using equations 17 and 18 (new) for six GAW stations (with the latitude and longitude for each station at the bottom right) with the shaded region representing the 25^{th} to 75^{th} percentiles. Observational data from 2014.

https://doi.org/10.5194/egusphere-2023-2447
Preprint. Discussion started: 17 November 2023

Variable	Definition	Constant / Dependance / Input
T	Sea surface temperature	Input
u_{10}	10 m wind speed	Input
u^*	friction velocity	u_{10}
u^*_w	waterside friction velocity	u_{10},u^*
C_D	drag coefficient	u_{10}
$[I^-]$	iodide concentration	Input
$[O_3]$	ozone concentration	Input
C_b	concentration in the bulk ocean	Input
S	Salinity	Input
C_a	concentration in the air	Input
κ	von Kármán constant	∼0.4
S_{cw}	Schmidt number in water	T,S
S_{ca}	Schmidt number in air	T
S_{c600}	Schmidt number of CO_2 at 20 °C	600
r_a	atmospheric resistance to dry deposition	u_{10}, u^*
r_b	quasilaminar sublayer resistance to dry deposition	u^*,S_{ca}
D	Diffusivity of O_3 in water	T
k	second-order rate coefficient of $O_3 + I^-$	T
a	chemical reactivity of $O_3 + I^-$	$[I^-]$,k
δ_m	depth of SML reaction-diffusion layer	a,D
α	solubility of O_3 in water	T
r_c	surface resistance to dry deposition	a,D,δ_m,κ,u^*_w,α
v_d	dry deposition velocity	r_a,r_b,r_c
H	unitless Henry's law	T,S
k_a	air-side transfer velocity	S_{ca},κ,u^*,C_D
k_w	water-side transfer velocity	u_{10},S_{cw},S_{c600}
R	surfactant scale factor	0.9
F_a	Net flux from the SML to the atmosphere	k_a,H,C_a,C_{sml}
F_b	Net flux (molecular transfer) from the SML to the bulk ocean	k_w,R,C_b,C_{sml}
F_r	Net flux (surface renewal) from the SML to the bulk ocean	u_{10},C_b,C_{sml}
C_{sml}	concentration in the SML	F_a,F_b,F_r

Table 1. All input variables and calculated parameters along with their definitions and dependencies used by the model presented in this work for calculating the dry deposition of O_3 into the SML and fluxes of inorganic halogens to the atmosphere and bulk ocean from the SML.

Continued on next page

https://doi.org/10.5194/egusphere-2023-2447
Preprint. Discussion started: 17 November 2023

Table 2 –*Continued from previous page*

Number	Reaction	Forward k	Reverse k	Reference

Table 2: All reactions included in the chemistry scheme of this SML model with forward and reverse rate constants (where applicable) and accompanying references. Numbered reactions with a and b denote different rates explored in the sensitivity analysis conducted in this paper. (1) A = 1.44×10^{22} $M^{-1}s^{-1}$, Ea = 73.08 kJ mol^{-1}, (2) A = 1.33×10^{10} $M^{-1}s^{-1}$, Ea = 8.5 kJ mol^{-1}, (3) assumed reaction based on theoretical calculation

Number	Reaction	Forward rate	Reverse rate	Reference
R1a	$O_3 + I^- \rightarrow$ IO-	(1)	NA	Magi et al. (1997)
R1b		(2)	NA	Brown et al. (2023)
R2	$I_2 \leftrightarrow I_2OH^- + H^+$	3.2	2.0×10^{10}	Lengyel et al. (1993)
R3	$I_2OH^- \leftrightarrow HOI + I^-$	1.34×10^{6}	4.0×10^{8}	Lengyel et al. (1993)
R4	$I^- + I_2 \leftrightarrow I_3^-$	6.2×10^{9}	8.9×10^{6}	Lengyel et al. (1993)
R5	$HOI + HOI \leftrightarrow H^+ + I^- + HIO_2$	25	2.0×10^{10}	Paquette (1989)
R6	$I_2 + OH^- \leftrightarrow HOI + I^-$	7.0×10^{4}	2.1×10^{3}	Sebők-Nagy and Körtvélyesi (2004)
R7	$HOI \leftrightarrow IO^- + H^+$	0.1	1×10^{10}	Paquette (1989)
R8	$HOI + IO^- \rightarrow HIO_2 + I^-$	15	NA	Bichsel and von Gunten (2000)
R9	$HIO_2 + HOI \leftrightarrow IO_3^- + I^- + 2H^+$	240	1.2×10^{3}	Paquette (1989)
R10	$H_2OI^+ \leftrightarrow HOI + H^+$	9.0×10^{8}	2.0×10^{10}	Lengyel et al. (1993)
R11	$I_2 + H_2O \leftrightarrow H_2OI^+ + I^-$	0.12	1.0×10^{10}	Lengyel et al. (1993)
R12	$HOI + Br^- + H^+ \leftrightarrow IBr$	4.1×10^{12}	8.0×10^{5}	De Barros Faria et al. (1993)
R13	$HOI + Cl^- + H^+ \leftrightarrow ICl$	2.9×10^{10}	2.4×10^{6}	Wang et al. (1989)
R14	$I_2 + Br^- \leftrightarrow I^- + IBr$	4.64×10^{3}	2.0×10^{9}	De Barros Faria et al. (1993)
R15a	$I_2 + Cl^- \leftrightarrow I_2Cl^-$	8.33×10^{4}	5.0×10^{4}	Kumar et al. (1986)
R15b		8.33×10^{4}	5.0×10^{3}	Schneider et al. (2023)
R16	$ICl_2^- \leftrightarrow ICl + Cl^-$	1.1×10^{9}	1.5	Kumar et al. (1986)
R17	$I^- + ICl \leftrightarrow I_2Cl^-$	1.1×10^{9}	1.5	Kumar et al. (1986)
R18(3)	$ICl_2^- + I^- \rightarrow I_2Cl^- + Cl^-$	1.0×10^{6}	NA	Kumar et al. (1986)
R19	$HOCl + I^- + H^+ \rightarrow ICl + H_2O$	3.5×10^{11}	NA	Nagy et al. (1988)
R20	$HOI + HOCl \rightarrow HIO_2 + Cl^- + H^+$	5.0×10^{5}	NA	Citri and Epstein (1988)
R21	$HIO_2 + HOCl \rightarrow IO_3^- + Cl^- + 2H^+$	1.5×10^{3}	NA	Lengyel et al. (1996)

Continued on next page

https://doi.org/10.5194/egusphere-2023-2447
Preprint. Discussion started: 17 November 2023

Table 2 –*Continued from previous page*

Number	Reaction	Forward k	Reverse k	Reference
R22	$Cl^- + O_3 + H^+ \rightarrow HOCl + O_2$	1.1×10^5	NA	Levanov et al. (2019)
R23	$Br^- + O_3 + H^+ \rightarrow HOBr + O_2$	11.7	NA	Haag and Hoigné (1983)
R24	$HOBr + Cl^- + H^+ \rightarrow BrCl + H_2O$	5.6×10^9	NA	Wang et al. (1994)
R25	$HOBr + Br^- + H^+ \rightarrow Br_2 + H_2O$	1.6×10^{10}	NA	Beckwith et al. (1996)
R26	$HOCl + Cl^- + H^+ \rightarrow Cl_2 + H_2O$	2.2×10^4	NA	Wang and Margerum (1994)
R27	$HOCl + Br^- + H^+ \rightarrow BrCl + H_2O$	1.3×10^6	NA	Kumar and Margerum (1987)
R28	$BrCl + H_2O \rightarrow HOBr + Cl^- + H^+$	1.0×10^5	NA	Wang et al. (1994)
R29	$Br_2 + H_2O \rightarrow HOBr + Br^- + H^+$	97	NA	Beckwith et al. (1996)
R30	$Cl_2 + H_2O \rightarrow HOCl + Cl^- + H^+$	22	NA	Wang and Margerum (1994)
R31[(3)]	$BrCl + Br^- \rightarrow Br_2Cl^-$	5.0×10^9	NA	Michalowski et al. (2000)
R32[(3)]	$Br_2 + Cl^- \rightarrow Br_2Cl^-$	5.0×10^9	NA	Michalowski et al. (2000)
R33[(3)]	$BrCl + Cl^- \rightarrow BrCl_2^-$	5.0×10^9	NA	Michalowski et al. (2000)
R34	$Br_2Cl^- \rightarrow Br_2 + Cl^-$	3.9×10^9	NA	Wang et al. (1994)
R35	$Br_2Cl^- \rightarrow BrCl + Br^-$	2.8×10^8	NA	Wang et al. (1994)
R36	$BrCl_2^- \rightarrow Cl_2 + Br^-$	690	NA	Wang et al. (1994)

https://doi.org/10.5194/egusphere-2023-2447
Preprint. Discussion started: 17 November 2023

Table 3. Comparison of I_2 emissions from published experimental studies with the SML model of this study, run using the experiment parameters. Model results were obtained with R=1, as no organics are present in these experimental results. a) pH 8 seawater spiked with iodide. b) pH 8 buffered solution with 0.5 M chloride and 1×10^{-6} M iodide. c) Artificial seawater containing iodide, bromide and chloride, buffered to pH 8. d) Iodide only in buffered pH 8. solution

Study	O_3 [ppbv]	Iodide [nM]	Stirred	Temperature [°C]	I_2 emission [molecules cm^{-2} s−1]	Model prediction [molecules cm^{-2} s−1]
Carpenter et al. (2013) [a]	70	10000-30000	Yes	18	0.6-1.8×10^{11}	0.2-0.3×10^{11}
MacDonald et al. (2014) [b]	222	1000	No	3-25	13±4×10^{9}	0.3-1.0×10^{9}
Tinel et al. (2020) [c]	20-110	1200	Yes	17	3-10×10^{8}	5.9-19×10^{8}
Tinel et al. (2020) [c]	34.7	400-10000	Yes	17	2-100×10^{8}	1.6-90×10^{8}
Schneider et al. (2023) [d]	95-110	390	No	22-25	7.7×10^{9}	0.1-0.6×10^{9}